

Big-Bang Nucleosynthesis Reactions Catalyzed by a Long-Lived Negatively-Charged Leptonic Particle

Masayasu KAMIMURA^{1,3}, Yasushi KINO² and Emiko HIYAMA³

¹ *Department of Physics, Kyushu University, Fukuoka 812-8581, Japan*

² *Department of Chemistry, Tohoku University, Sendai 980-8578, Japan*

³ *RIKEN Nishina Center, RIKEN, Wako, Saitama 351-0198, Japan*

Accurate quantum three-body calculation is performed for the new rank of big-bang nucleosynthesis (BBN) reactions that are catalyzed by a hypothetical long-lived negatively-charged, massive leptonic particle (called X^-) such as a supersymmetric (SUSY) particle *stau*, the scalar partner of the tau lepton. It is known that if the X^- particle has a lifetime of $\tau_X \gtrsim 10^3$ s, it would capture a light element previously synthesized in standard BBN and form a Coulombic bound state, for example, (${}^7\text{Be}X^-$) at temperature $T_9 \lesssim 0.4$ (in units of 10^9 K), (αX^-) at $T_9 \lesssim 0.1$ and (pX^-) at $T_9 \lesssim 0.01$. The bound state, an exotic atom, is expected to induce the following reactions in which X^- works as a catalyzer: i) α -transfer reactions such as $(\alpha X^-) + d \rightarrow {}^6\text{Li} + X$, ii) radiative capture reactions such as $({}^7\text{Be}X^-) + p \rightarrow ({}^8\text{B}X^-) + \gamma$, iii) three-body breakup reactions such as $({}^7\text{Li}X^-) + p \rightarrow \alpha + \alpha + X^-$, iv) charge-exchange reactions such as $(pX^-) + \alpha \rightarrow (\alpha X^-) + p$, and v) neutron induced reactions such as $({}^8\text{Be}X^-) + n \rightarrow {}^9\text{Be} + X^-$. Recent literature papers have claimed that some of these X^- -catalyzed reactions have significantly large cross sections so that inclusion of the reactions into the BBN network calculation can change drastically abundances of some elements, giving not only a solution to the ${}^6\text{Li}$ - ${}^7\text{Li}$ problem (calculated underproduction of ${}^6\text{Li}$ by ~ 1000 times and overproduction of ${}^7\text{Li}$ + ${}^7\text{Be}$ by ~ 3 times) but also a constraint on the lifetime and the primordial abundance of the elementary particle X^- . However, most of these literature calculations of the reaction cross sections were made assuming too naive models or approximations that are unsuitable for those complicated low-energy nuclear reactions. We use a high-accuracy few-body calculational method developed by the authors, and provides precise cross sections and rates of those catalyzed BBN reactions for the use in the BBN network calculation.

§1. Introduction

Accurate theoretical prediction of nuclear reaction rates is essentially important in the study of big-bang nucleosynthesis (BBN) when particular reaction rates are very hard or even impossible to estimate experimentally. The most typical example of such reactions is production and destruction of light elements being catalyzed by a hypothetical long-lived negatively-charged massive ($\gtrsim 100$ GeV) leptonic particle, here denoted as X^- ; a candidate is the supersymmetric (SUSY) counterpart of a tau lepton (τ), i.e., a stau ($\tilde{\tau}$)^{*}. Recently, BBN involving those X^- -catalyzed nuclear reactions has extensively been studied from the viewpoint of particle-physics catalysis in BBN,¹⁾⁻¹⁴⁾ which may be shortly reviewed as follows (precisely reviewed in Refs. 12), 14) and more references therein):

i) If the X^- particle has a lifetime of the order of 10^3 s or longer, it would capture a light nucleus, A , previously synthesized during BBN and produce a bound state denoted as (AX^-) , which is a kind of exotic atom with the nucleus A in a Coulombic

^{*}) Stau is one of the particles expected to be discovered at CERN Large Hadron Collider.¹⁶⁾

orbit around the massive X^- at the center.*)

ii) When the cosmic temperature cools to $T_9 \sim 0.4$ (in units of 10^9 K) after the standard BBN ($T_9 \gtrsim 0.5$), X^- captures ${}^7\text{Be}$ to form (${}^7\text{Be}X^-$) which is subsequently destroyed by the (${}^7\text{Be}X^-$) + $p \rightarrow ({}^8\text{B}X^-) + \gamma$ reaction⁶⁾ followed by the β -decay of (${}^8\text{B}X^-$) to $\alpha + \alpha + X^-$.

iii) At the temperature $T_9 \sim 0.3$, X^- catches ${}^7\text{Li}$ to generate (${}^7\text{Li}X^-$) which is subsequently destroyed by the (${}^7\text{Li}X^-$) + $p \rightarrow \alpha + \alpha + X^-$ reaction.

iv) At $T_9 \sim 0.1$, X^- particles capture α particles to form abundant (αX^-) which triggers (αX^-) + $d \rightarrow {}^6\text{Li} + X^-$ to produce enormous amount of ${}^6\text{Li}$, as originally proposed by Pospelov¹⁾ and confirmed by Hamaguchi *et al.*⁵⁾ including the two of the present authors (M.K. and Y.K.).

v) At $T_9 \sim 0.01$, although X^- particles start capturing protons to form (pX^-), its abundance remains low due to the (pX^-) + $\alpha \rightarrow (\alpha X^-) + p$ reaction which operates before (pX^-) begins frequent interactions with other nuclei to make heavier elements.¹⁴⁾

Contribution of those reactions is expected to modify standard BBN (SBBN in short) and to solve the calculated underproduction (~ 1000 times) of the primordial abundance of ${}^6\text{Li}$ and the overproduction (~ 3 times) of ${}^7\text{Li}$,¹⁵⁾ and, at the same time, to provide with information for constraining the lifetime and the primordial abundance of the elementary particle X^- . However, studies of the reactions, except for the work of Ref. 5) on the ${}^6\text{Li}$ production, have not been performed fully quantum mechanically on the basis of the nuclear reaction theory.

The purpose of the present paper is to perform a precise quantum three-body calculation of the cross sections of many kinds of catalyzed BBN (CBBN in short) reactions including the ones mentioned above in i) - v) and to provide their reaction rates for the use in the BBN network calculation. The adopted theoretical method and numerical technique has been developed by the present authors, reviewed in Ref. 18), and is well established in the field of few-body atomic and nuclear systems.

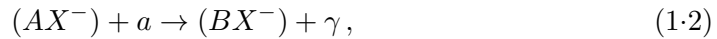
CBBN reactions studied in this paper are classified into four types:

1) *Transfer reactions:*

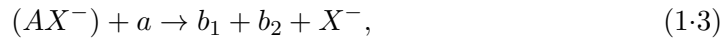


where A is picked up by an incoming nucleus a to produce a nucleus $B (= A + a)$,

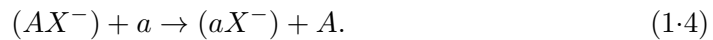
2) *Radiative capture reactions:*



3) *Three-body breakup reactions:*



4) *Charge-exchange reactions:*



*) For instance, binding energies of (${}^7\text{Be}X^-$) and (αX^-) are ~ 1.3 MeV and ~ 0.34 MeV, and r.m.s. radii are ~ 3.6 fm and ~ 7 fm, respectively.

We solve the Schrödinger equations of the CBBN reactions (1.1)–(1.4) taking explicitly the three-body degree of freedom into account and derive their cross sections and reaction rates at incoming energies below 200 keV.

Throughout this paper, it is not necessary to identify X^- with any particular particle such as the SUSY particle stau though it was assumed, for instance, in Refs.4), 5), 14). The property of X^- we assume here is that X^- has a charge $-e$, a mass $m_X \gtrsim 100$ GeV and a lifetime $\tau_X \gtrsim 10^3$ s and that X^- interacts with light elements via the Coulomb force only.

Construction of the present paper is as follows: We investigate X^- -catalyzed α -transfer reactions to produce ${}^6\text{Li}$, ${}^7\text{Li}$ and ${}^7\text{Be}$ in §2, resonant and non-resonant radiative capture reactions to destroy ${}^7\text{Be}$ in §3, three-body breakup reactions to destroy ${}^6\text{Li}$ and ${}^7\text{Li}$ in §4, the charge-exchange reactions in §5 and a possibility of X^- -catalyzed primordial production of ${}^9\text{Be}$ in §6. Summary is given in §7.

§2. X^- -catalyzed α -transfer reactions

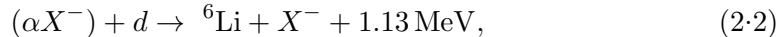
2.1. Necessity of three-body calculation

2.1.1. Production of ${}^6\text{Li}$

One of the puzzles in SBBN is that the BBN prediction of the ${}^6\text{Li}$ abundance lies a factor of ~ 1000 smaller than the observed data.¹⁵⁾ The too small prediction is mostly because the radiative capture reaction to produce ${}^6\text{Li}$ in SBBN,



is heavily E1-hindered with a very small astrophysical S -factor, $S_\gamma \sim 2 \times 10^{-6}$ keV b.¹⁷⁾ In order to obtain much more production of ${}^6\text{Li}$, Pospelov proposed,¹⁾ for the first time, to consider a new type of CBBN reaction,



in which the bound state*) (αX^-) works to synthesize α and d to form ${}^6\text{Li}$ with no photon emitting. He claimed that the S -factor of the X^- -catalyzed reaction (2.2), say S_X , is enhanced by 8 order of magnitude ($S_X \sim 3 \times 10^2$ keV b) compared with S_γ , and the abundance of ${}^6\text{Li}$ is very much increased so that the ${}^6\text{Li}$ problem can be solved under a proper restriction on the abundance and the lifetime of X^- .

His estimation of S_X , however, was based on a too naive comparison between (2.1) and (2.2). Namely, in an analogy to the real photon in (2.1) with the wavelength $\lambda_\gamma \sim 130$ fm, Pospelov introduced a virtual photon in (2.2) with a characteristic wavelength λ_X on the order of the Bohr radius (= 3.63 fm) of the atom (αX^-) and assumed a scaling relation**)

$$\frac{S_X}{S_\gamma} \sim \left(\frac{\lambda_\gamma}{\lambda_X} \right)^{2\ell+1}, \quad (2.3)$$

*) When (αX^-) is in the $1s$ ground state, the suffix $1s$ of $(\alpha X^-)_{1s}$ is omitted hereafter.

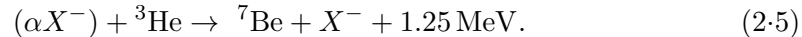
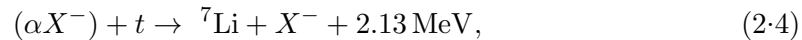
**) More detailed expression is given by Eq.(4) in Ref. 1) but is essentially described by (2.3).

where the photon multipolarity ℓ is assumed to be $\ell = 2$ (namely, E2) not only for the real photon^{*)} but also for the virtual one. The enhancement ratio S_X/S_γ amounts to $\sim 10^8$.

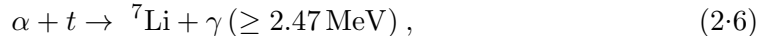
But, the scaling relation (2·3) which compares the wavelengths of the real and virtual photons is not suitable for discussing the reaction (2·2) because the relation does not take into account the nuclear interaction that is the most important factor in the process to transfer the α particle from (αX^-) to the deuteron to form ${}^6\text{Li}$. Therefore, two of the authors (M.K. and Y.K.) and their collaborators⁵⁾ performed a fully-quantum three-body calculation of the $\alpha + d + X^-$ system and calculated the S -factor of the reaction (2·2), $S_X(E)$, as a function of the incident c.m. energy E at $E = 10 - 120$ keV. The calculated S -factor at the Gamow-peak energy is 38 keV b ($S_X/S_\gamma \sim 10^7$, nearly one-order of magnitude smaller than that in Ref. 1)). Note that S_X of the CBBN reaction (2·2) is in a similar order of magnitude compared with S -factors of non-resonant photonless SBBN reactions caused by the nuclear interaction; for example, compare the S_X with observed values of ~ 60 keV b for $d + d \rightarrow t + p$ and $\sim 5 \times 10^{-6}$ keV b for the E1-forbidden process $d + d \rightarrow \alpha + \gamma$. The large enhancement of the CBBN/SBBN ratio ($\sim 10^7$) is simply because the SBBN reaction (2·1) is heavily E1-hindered.

2.1.2. Production of ${}^7\text{Li}$ and ${}^7\text{Be}$

In the BBN network calculation with the CMB-based baryon-to-photon ratio,¹⁹⁾ $\eta_B = 6.0 \times 10^{-10}$, abundance of ${}^7\text{Be}$ is approximately one order of magnitude larger than that of ${}^7\text{Li}$. Since ${}^7\text{Be}$ eventually decays to ${}^7\text{Li}$ by electron capture, sum of both the abundances of ${}^7\text{Li}$ and ${}^7\text{Be}$ is regarded as the abundance of ${}^7\text{Li}$ in the ${}^7\text{Li}$ -overproduction problem. In order to examine the effect of CBBN on the abundance of ${}^7\text{Li}+{}^7\text{Be}$, Cyburt *et al.*⁴⁾ studied the α -transfer reactions,



which produce ${}^7\text{Li}$ and ${}^7\text{Be}$ at $T_9 \sim 0.1$. Using the scaling relation proposed in Ref. 1), they claimed that the S -factors of the above CBBN reactions are 5 orders of magnitude greater than those of the E1 radiative capture reactions,



that are the most effective source to produce ${}^7\text{Li}$ and ${}^7\text{Be}$ in SBBN.

However, it is clear that the enhancement ratio CBBN/SBBN in S -factors will be only the order of $10^1 - 10^2$ contrary to the case of the ${}^6\text{Li}$ production ($\sim 10^7$). The reason is as follows: SBBN S -factors of (2·6) and (2·7) at astrophysical energies are

^{*)} This particular assumption of $\ell = 2$ for the real photon in (2·1) may not be justified at *astrophysical energies* (no experimental data there). According to the so-far most precise six-body calculation²⁰⁾ of the E1-hindered radiative capture reaction (2·1), S -factor of the E2 transition decreases much more rapidly than that of E1 as the energy decreases, and eventually the E1/E2 ratio becomes ~ 10 at $E \sim 0$ (see Figs.7 and 8 of Ref. 20)).

respectively ~ 0.1 keV b and ~ 0.5 keV b¹⁷⁾ which are 5 orders of magnitude larger than that of the E1-hindered reaction (2.1). Moreover, CBBN S -factors of (2.4) and (2.5) should be much reduced compared with that of (2.2), because rearrangement of the angular momenta among the three particles is needed when going from the entrance channel to the exit one; note that a significant difference between (2.2) and (2.4)–(2.5) is that the relative motion between d and α in ${}^6\text{Li}$ is of s -wave whereas that between $t({}^3\text{He})$ and α in ${}^7\text{Li}$ (${}^7\text{Be}$) is of p -wave. This consideration on the CBBN/SBBN ratio will be confirmed by the quantum three-body calculation of (2.4) and (2.5) in this section.

2.2. Three-body Schrödinger equation and reaction rate

Following Refs. 5), 18), we briefly explain the three-body calculational method to investigate the X^- -catalyzed transfer reactions above. It is to be emphasized that the method described here is an exact method to calculate the cross section of the low-energy transfer reactions within the three-body model of the total system concerned. The present authors have an experience of performing the same types of calculations in the study of muon-transfer reactions^{18), 21)–23)} seen in the muon-catalyzed fusion cycles.²⁴⁾

As shown in Fig. 1, we consider all the three sets of the Jacobi coordinates ($\mathbf{r}_c, \mathbf{R}_c$), $c = 1, 2$ and 3, in order to treat completely the three-body degrees of freedom of the system $A + a + X^-$. Here, we take $A = \alpha$ and $a = d, t$ and ${}^3\text{He}$ for the reactions (2.2), (2.4) and (2.5), respectively.

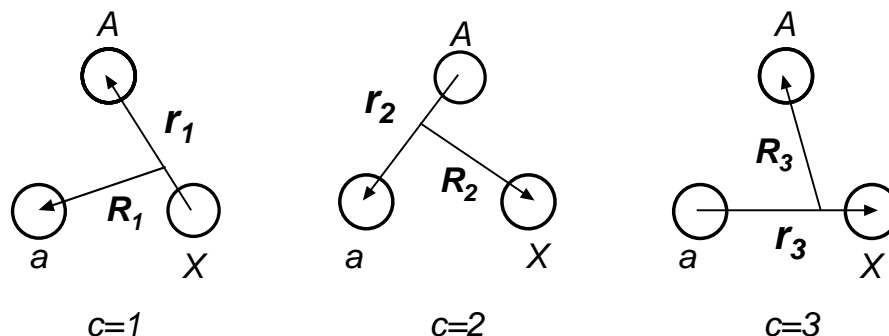


Fig. 1. Three sets of Jacobi coordinates of the $A+a+X^-$ system. The entrance channel $(AX^-)+a$ is described by using the coordinate system $c = 1$, and the transfer channels $(Aa)+X^-$ by $c = 2$ and $(aX^-)+A$ by $c = 3$.

The Schrödinger equation for the total wave function having an total energy E_{tot} and an angular momentum J and its z -component M is given by

$$(H - E_{\text{tot}})\Psi_{JM} = 0 \quad (2.8)$$

with the Hamiltonian,

$$H = -\frac{\hbar^2}{2m_c}\nabla_{\mathbf{r}_c}^2 - \frac{\hbar^2}{2M_c}\nabla_{\mathbf{R}_c}^2 + V_{A-X}(r_1) + V_{A-a}(r_2) + V_{a-X}(r_3). \quad (2.9)$$

As far as we use the reduced masses (m_c and M_c) associated with the coordinates (\mathbf{r}_c and \mathbf{R}_c), every choice of c in the kinetic term is equivalent. Notation of the potentials is self-evident; explicit form will be given below. The Schrödinger equation is solved under the scattering boundary condition imposed appropriately on the reaction concerned.

Throughout all the CBBN reactions studied in this paper, only the resonant radiative capture reaction (1·2) requires serious consideration on intrinsic spins of the particles as will be discussed in §3. In this section for the non-resonant α -transfer reactions, spin of the incoming particle $a(= d, t, {}^3\text{He})$ is neglected. Therefore, in the exit channel of (2·4) and (2·5), the $3/2^-$ (p -wave) ground state and the $1/2^-$ (p -wave) first excited state of ${}^7\text{Li}$ and ${}^7\text{Be}$ are degenerated energetically to their weighted mean. How good is this approximation will be presented in §2.6.

Firstly, we construct the wave function of the $1s$ ground state of (AX^-) in the entrance channel on the coordinate system $c = 1$ and that of the ground state of the nucleus B on $c = 2$. We denote the wave function by $\phi_{l_c m_c}^{(c)}(\mathbf{r}_c)$ and the eigenenergy by $\varepsilon_{l_c}^{(c)}$; explicitly, $l_1 = 0$ for (αX^-) , $l_2 = 0$ for ${}^6\text{Li}$ and $l_2 = 1$ for ${}^7\text{Li}$ (${}^7\text{Be}$). Those quantities are obtained by solving

$$\left[-\frac{\hbar^2}{2m_c} \nabla_{\mathbf{r}_c}^2 + V_c(r_c) - \varepsilon_{l_c}^{(c)} \right] \phi_{l_c m_c}^{(c)}(\mathbf{r}_c) = 0, \quad (c = 1, 2) \quad (2\cdot10)$$

where the potential V_c denotes V_{A-X} and V_{A-a} for $c = 1$ and 2 , respectively.

By $\chi_{L_c M_c}^{(c)}(\mathbf{R}_c) \equiv \chi_{L_c}^{(c)}(R_c) Y_{L_c M_c}(\widehat{\mathbf{R}}_c)$ we denote the scattering wave function along the coordinate \mathbf{R}_c with the angular momentum L_c and its z -component M_c ($c = 1, 2$). The center-of-mass (c.m.) scattering energy associated with the coordinate \mathbf{R}_c , say E_c , is introduced by

$$E_c = E_{\text{tot}} - \varepsilon_{l_c}^{(c)} = \hbar^2 k_c^2 / 2M_c \quad (c = 1, 2) \quad (2\cdot11)$$

together with the corresponding wave number k_c .

The total three-body wave function Ψ_{JM} which describes the transfer reaction (2·2) in the most sophisticated manner is written as^{18),25)}

$$\Psi_{JM} = \phi_{00}^{(1)}(\mathbf{r}_1) \chi_{JM}^{(1)}(\mathbf{R}_1) + \left[\phi_{l_2}^{(2)}(\mathbf{r}_2) \otimes \chi_{L_2}^{(2)}(\mathbf{R}_2) \right]_{JM} + \Psi_{JM}^{(\text{closed})}. \quad (2\cdot12)$$

Here, the first and the second terms represent the two open channels, $(AX^-) + a$ on $c = 1$ and $B + X^-$ on $c = 2$, respectively; there are no other open channels in the energy range ($E_1 < 150$ keV) we are interested in. In the first term, the radial part $\chi_J^{(1)}(R_1)$ has incoming and outgoing amplitudes, and $\chi_{L_2}^{(2)}(R_2)$ in the second term has the outgoing amplitude only. They should satisfy the boundary condition:

$$\lim_{R_c \rightarrow \infty} R_c \chi_{L_c}^{(c)}(R_c) = u_{L_c}^{(-)}(k_c, R_c) \delta_{c1} - \sqrt{\frac{v_1}{v_c}} S_{1 \rightarrow c}^{L_c} u_{L_c}^{(+)}(k_c, R_c), \quad (c = 1, 2) \quad (2\cdot13)$$

where $L_1 = J$, and $u_L^{(\pm)}(k_c R_c) (= G_L(k_c R_c) \pm i F_L(k_c R_c))$ are the asymptotic outgoing and incoming Coulomb wave functions. $S_{1 \rightarrow c}^{L_c}$ is the S-matrix for the transition from the incoming channel ($c = 1$) to the outgoing channel c and v_c is the velocity.

The third term in (2.12), $\Psi_{JM}^{(\text{closed})}$, stands for all the closed (virtually-excited) channels in the energy range of this work; in other words, this term is responsible for all the asymptotically-vanishing amplitudes due to the three-body degrees of freedom that are not included in the first two scattering terms.*). Since $\Psi_{JM}^{(\text{closed})}$ vanishes asymptotically, it is reasonable and useful to expand it in terms of a complete set of L^2 -integrable three-body basis functions, $\{\Phi_{JM,\nu}; \nu = 1 - \nu_{\text{max}}\}$, that are spanned in a finite spatial region (see §2.4):

$$\Psi_{JM}^{(\text{closed})} = \sum_{\nu=1}^{\nu_{\text{max}}} b_{J\nu} \Phi_{JM,\nu}. \quad (2.14)$$

Equations for $\chi_J^{(1)}(R_1)$, $\chi_{L_2}^{(2)}(R_2)$ and the coefficients $b_{J\nu}$ are given by the $\nu_{\text{max}} + 2$ simultaneous equations,^{18),25)}

$$\langle \phi_{00}^{(1)}(\mathbf{r}_1) Y_{JM}(\widehat{\mathbf{R}}_1) | H - E_{\text{tot}} | \Psi_{JM} \rangle_{\mathbf{r}_1, \widehat{\mathbf{R}}_1} = 0, \quad (2.15)$$

$$\langle [\phi_{l_2}^{(2)}(\mathbf{r}_2) \otimes Y_{L_2}(\widehat{\mathbf{R}}_2)]_{JM} | H - E_{\text{tot}} | \Psi_{JM} \rangle_{\mathbf{r}_2, \widehat{\mathbf{R}}_2} = 0, \quad (2.16)$$

and

$$\langle \Phi_{JM,\nu} | H - E_{\text{tot}} | \Psi_{JM} \rangle = 0. \quad (\nu = 1 - \nu_{\text{max}}) \quad (2.17)$$

Here, $\langle \rangle_{\mathbf{r}_c, \widehat{\mathbf{R}}_c}$ denotes the integration over \mathbf{r}_c and $\widehat{\mathbf{R}}_c$.

Since $\Phi_{JM,\nu}$ are constructed so as to diagonalize the three-body Hamiltonian as (cf. §2.4)

$$\langle \Phi_{JM,\nu} | H | \Phi_{JM,\nu'} \rangle = E_{J\nu} \delta_{\nu\nu'}, \quad (\nu, \nu' = 1 - \nu_{\text{max}}) \quad (2.18)$$

the coefficients $b_{J\nu}$ can be written, from Eq.(2.17), as

$$b_{J\nu} = \frac{-1}{E_{J\nu} - E_{\text{tot}}} \langle \Phi_{JM,\nu} | H - E_{\text{tot}} | \phi_{00}^{(1)}(\mathbf{r}_1) \chi_{JM}^{(1)}(\mathbf{R}_1) + [\phi_{l_2}^{(2)}(\mathbf{r}_2) \otimes \chi_{L_2}^{(2)}(\mathbf{R}_2)]_{JM} \rangle. \quad (\nu = 1 - \nu_{\text{max}}) \quad (2.19)$$

Inserting Eqs.(2.19) into $b_{J\nu}$ in Ψ_{JM} in Eqs.(2.15) and (2.16), we reach two coupled integro-differential equations for $\chi_J^{(1)}(R_1)$ and $\chi_J^{(2)}(R_2)$, though not written here (see §8 of Ref. 18) for them).

Finally, the integro-differential equations are solved using both the direct numerical method (the finite-difference method) and the Kohn-type variational method.^{18),25)} We have obtained the same result; this demonstrates the high accuracy of our three-body calculation.

By using the S -matrix elements obtained above, the cross section of the rearrangement process is expressed as

$$\sigma(E) = \frac{\pi}{k_1^2} \sum_{J=0}^{\infty} (2J+1) |S_{1 \rightarrow 2}^{L_2}|^2. \quad (2.20)$$

*) This method for low-energy three-body reactions has already been used^{18),21)-23)} in the study of the muon transfer reaction $(d\mu)_{1s} + t \rightarrow (t\mu)_{1s} + d + 48 \text{ eV}$. The $\Psi_{JM}^{(\text{closed})}$ term was found to play a very important role; if the term is omitted (namely if the two-channel coupled calculation is performed with $c = 1, 2$), the calculated low-energy (0.001 – 100 eV) cross section of the reaction becomes ~ 30 times larger than that obtained by the full three-body calculation.

where we introduce a simplified notation, $E \equiv E_1$, for the energy of the entrance channel. The astrophysical S -factor is derived from

$$\sigma(E) = S(E) \exp(-2\pi\eta(E))/E. \quad (2.21)$$

Here, $\exp(-2\pi\eta(E))$ is the Coulomb-barrier penetration probability, $\eta(E)$ being the Sommerfeld parameter of the entrance channel (AX^-) + a defined as

$$\eta(E) = Z_a Z_{AX} e^2 / \hbar v_1, \quad (2.22)$$

where $Z_a e$ and $Z_{AX} e$ are the charges of a and (AX^-), respectively.

The reaction rate $\langle \sigma v \rangle$ at a temperature T is expressed as (cf. Eq.(4-44) of Ref. 26))

$$\langle \sigma v \rangle = \left(\frac{8}{\pi M_1} \right)^{\frac{1}{2}} \frac{1}{(kT)^{\frac{3}{2}}} \int_0^\infty S(E) \exp\left(-\frac{E}{kT} - 2\pi\eta(E)\right) dE, \quad (2.23)$$

where k is the Boltzmann constant. If $S(E)$ is simulated by a linear function of E around the Gamow-peak energy E_0 as

$$S(E) \simeq S(E_0) + \left(\frac{\partial S}{\partial E} \right)_{E_0} (E - E_0), \quad (2.24)$$

$$E_0 = 122.0 (Z_a^2 Z_{AX}^2 \mu)^{\frac{1}{3}} T_9^{\frac{2}{3}} \text{ keV}, \quad (2.25)$$

the reaction rate $N_A \langle \sigma v \rangle$ is expressed, using Eqs.(4-56) and (4-75) of Ref. 26), as

$$\begin{aligned} N_A \langle \sigma v \rangle &= 7.82 \times 10^6 \left(\frac{Z_a Z_{AX}}{\mu} \right)^{\frac{1}{3}} \left[S(E_0) + 71.8 \left(\frac{\partial S}{\partial E} \right)_{E_0} T_9 \right] \\ &\times T_9^{-\frac{2}{3}} \exp \left[-4.248 (Z_a^2 Z_{AX}^2 \mu)^{\frac{1}{3}} T_9^{-\frac{1}{3}} \right] \text{ cm}^3 \text{ s}^{-1} \text{ mol}^{-1}, \quad (2.26) \end{aligned}$$

where $S(E_0)$ and $(\partial S/\partial E)_{E_0}$ are to be given in units of keV b and b, respectively, N_A being the Avogadro's number and μ being M_1 in units of amu. As will be seen in any non-resonant reaction in this paper, we can regard $(\partial S/\partial E)_{E_0} \approx \text{constant} \equiv \alpha$:

$$S(E) = S(E_0) + \alpha (E - E_0) = S(0) + \alpha E, \quad (2.27)$$

where $S(0)$ and α is given in units of keV b and b, E being in keV. We then have

$$\begin{aligned} N_A \langle \sigma v \rangle &= 7.82 \times 10^6 \left(\frac{Z_a Z_{AX}}{\mu} \right)^{\frac{1}{3}} S(0) T_9^{-\frac{2}{3}} \exp \left[-4.248 (Z_a^2 Z_{AX}^2 \mu)^{\frac{1}{3}} T_9^{-\frac{1}{3}} \right] \\ &\times \left[1 + \frac{\alpha}{S(0)} \left\{ 122.0 (Z_a^2 Z_{AX}^2 \mu)^{\frac{1}{3}} T_9^{\frac{2}{3}} + 71.8 T_9 \right\} \right] \text{ cm}^3 \text{ s}^{-1} \text{ mol}^{-1}. \quad (2.28) \end{aligned}$$

2.3. Nuclear and Coulomb potentials

It is essential in the three-body calculation to employ appropriate interactions among the three particles. Here, we determine the potentials $V_{A-X}(r_1)$, $V_{A-a}(r_2)$ and $V_{a-X}(r_3)$ in (2.9) where $A = \alpha$ and $a = d, t$ and ${}^3\text{He}$.

We assume Gaussian-shape charge distribution $Ze(\pi b^2)^{-3/2}e^{-(r/b)^2}$ for α , d , t and ${}^3\text{He}$; here, Ze is the charge and $b = \sqrt{2/3}r_0$, r_0 being the observed r.m.s. charge radius which is given by $r_0 = 1.67$ fm, 2.14 fm, 1.70 fm and 1.95 fm, respectively.

The Coulomb potential between A and X^- is given by

$$V_{A-X}(r) = -Z_A e^2 \frac{\text{erf}(r/b_A)}{r}, \quad (2.29)$$

where $\text{erf}(x) = \frac{2}{\sqrt{\pi}} \int_0^x e^{-t^2} dt$ is the error function; and similarly for $V_{a-X}(r)$. Energy of the $(\alpha X^-)_{1s}$ state is $\varepsilon_{\text{g.s.}}^{(1)} = -337.3$ keV (-347.6 keV) and the r.m.s. radius is 6.84 fm (6.69 fm) for $m_X = 100$ GeV ($m_X \rightarrow \infty$).

The potential $V_{A-a}(r)$ is a sum of the nuclear potential, $V_{A-a}^{\text{N}}(r)$, and the Coulomb one, $V_{A-a}^{\text{C}}(r)$. The latter is given by

$$V_{A-a}^{\text{C}}(r) = Z_A Z_a e^2 \frac{\text{erf}(r/\sqrt{b_A^2 + b_a^2})}{r}. \quad (2.30)$$

The nuclear potential $V_{A-a}^{\text{N}}(r)$ is assumed to have a two-range Gaussian shape as

$$V_{A-a}^{\text{N}}(r) = v_1 e^{-(r/a_1)^2} + v_2 e^{-(r/a_2)^2}. \quad (2.31)$$

i) $\alpha - d$ potential

We take $a_1 = 0.9$ fm, $v_1 = 500.0$ MeV, $a_2 = 2.0$ fm and $v_2 = -64.06$ MeV.⁵⁾ The first term, a repulsive core, is introduced to simulate the Pauli exclusion principle that nucleons in the incoming deuteron should not occupy the nucleon s -orbit in the α particle during the reaction process (for this role of Pauli principle,^{*} see e.g. Ref. 27)). The parameters are so determined that the solution to the Schrödinger equation (2.10) for $c = 2$ reproduces observed values of the energy $\varepsilon_{\text{g.s.}}^{(2)} = -1.474$ MeV and the r.m.s. charge radius 2.54 fm³³⁾ of the ground state of ${}^6\text{Li}$. Furthermore, the charge density of ${}^6\text{Li}$ reproduces the observed charge form factor of the electron scattering from ${}^6\text{Li}$ (see Fig. 2a of Ref. 5)). Simultaneously, use of the potential $V_{\alpha-d}(r_2)$ explains the low-energy s -wave phase shifts of the $\alpha + d$ scattering (see Fig. 2b of Ref. 5)).

ii) $\alpha - t$ potential

The nuclear potential between α and t is assumed to be parity dependent; $a_1 = 1.0$ fm, $v_1 = 500.0$ MeV, $a_2 = 2.7$ fm and $v_2 = -46.22$ MeV for odd angular-momentum

^{*} Use of the sophisticated orthogonality-condition model (OCM)²⁸⁾ for three-body systems is not necessary in the present case, since the Pauli principle works only between A and a among the three particles, and we are not treating compact bound states of them. But, introduction of the inner repulsive potential is useful in this type of three-body scattering calculation to prevent automatically the unphysical Pauli forbidden amplitude from the total wave function.

states and $a_1 = 1.5$ fm, $v_1 = 500.0$ MeV, $a_2 = 2.4$ fm and $v_2 = -7.0$ MeV for even angular-momentum states. The repulsive term is introduced so as to prevent the Pauli-forbidden states from mixing into the total wave function. Use of the potential reproduces the observed energy $\varepsilon_{\text{g.s.}}^{(2)} = -2.308$ MeV (weighted average for the $3/2^-$ ground state and the $1/2^-$ excited state) and the r.m.s. charge radius 2.43 fm³³⁾ of the ground state of ${}^7\text{Li}$ as well as observed values of the low-energy $\alpha - t$ scattering phase shifts for the p -wave (average of the $p_{3/2}$ and $p_{1/2}$ states) and the s -wave.

iii) $\alpha - {}^3\text{He}$ potential

The nuclear $\alpha - {}^3\text{He}$ potential is assumed to have the same shape and parameters as the $\alpha - t$ potential but for $v_2 = -44.84$ MeV for odd states, which reproduces the observed weighted mean energy ($\varepsilon_{\text{g.s.}}^{(2)} = -1.444$ MeV) of the ground state and the $1/2^-$ excited state.

2.4. Three-body basis functions

The L^2 -integrable three-body basis functions $\{\Phi_{JM,\nu}; \nu = 1 - \nu_{\text{max}}\}$ used in (2.14) to expand $\Psi_{JM}^{(\text{closed})}$ are introduced as follows:¹⁸⁾ $\Phi_{JM,\nu}$ are written as a sum of the component functions in the Jacobi-coordinate sets $c = 1 - 3$ (Fig. 1),

$$\Phi_{JM,\nu} = \Phi_{JM,\nu}^{(1)}(\mathbf{r}_1, \mathbf{R}_1) + \Phi_{JM,\nu}^{(2)}(\mathbf{r}_2, \mathbf{R}_2) + \Phi_{JM,\nu}^{(3)}(\mathbf{r}_3, \mathbf{R}_3). \quad (2.32)$$

Each component is expanded in terms of the Gaussian basis functions of \mathbf{r}_c and \mathbf{R}_c :

$$\Phi_{JM,\nu}^{(c)}(\mathbf{r}_c, \mathbf{R}_c) = \sum_{n_c l_c, N_c L_c} A_{J\nu, n_c l_c, N_c L_c}^{(c)} [\phi_{n_c l_c}^{\text{G}}(\mathbf{r}_c) \psi_{N_c L_c}^{\text{G}}(\mathbf{R}_c)]_{JM} \quad (c = 1 - 3), \quad (2.33)$$

where the Gaussian ranges are postulated to lie in geometric progression:

$$\phi_{nlm}^{\text{G}}(\mathbf{r}) = r^l e^{-(r/r_n)^2} Y_{lm}(\hat{\mathbf{r}}), \quad r_n = r_1 a^{n-1}, \quad (n = 1 - n_{\text{max}}) \quad (2.34)$$

$$\psi_{NLM}^{\text{G}}(\mathbf{R}) = R^L e^{-(R/R_N)^2} Y_{LM}(\hat{\mathbf{R}}), \quad R_N = R_1 A^{N-1}. \quad (N = 1 - N_{\text{max}}) \quad (2.35)$$

Basis functions so chosen are suited for describing both short range correlations (mainly due to nuclear interactions) and long range asymptotic behavior simultaneously, and therefore they are efficient to describe any three-body configuration (the closed-channel contribution) in the interaction region of the intermediate stage of reactions. The coefficients $A_{J\nu, n_c l_c, N_c L_c}^{(c)}$ in (2.33) and the eigenenergies $E_{J,\nu}$ of $\Phi_{JM,\nu}$ are determined by diagonalizing the three-body Hamiltonian H as (2.18).

This method in which the total Hamiltonian is diagonalized by using the precise Gaussian basis functions has successfully been applied to the study of various types of three- and four-body systems in physics^{*)}, which is reviewed in Ref. 18).

i) Basis set for $\alpha + d + X^-$

*) The most precise calculation among them is the determination^{18), 29)} of the antiproton mass³⁰⁾ by analyzing the CERN's laser spectroscopic data on the antiprotonic helium atom, $\text{He}^{++} + e^- + \bar{p}$.³¹⁾ Energies of the three-body atom with $J \sim 35$ was calculated with the accuracy of 10 significant figures.

In the calculation for $J = 0$, we took $l_c = L_c = 0, 1, 2$ and $n_{\max} = N_{\max} = 15$ for $c = 1 - 3$. Then, total number of the three-body Gaussian basis $[\phi_{n_c l_c}^G(\mathbf{r}_c) \psi_{N_c L_c}^G(\mathbf{R}_c)]_{JM}$ to construct $\{\Phi_{JM, \nu}\}$ amounts to $\nu_{\max} = 2025$, which was found to be large enough for the present calculation. As for the Gaussian ranges, we took $\{r_1, r_{n_{\max}}, R_1, R_{N_{\max}}\} = \{0.5, 15.0, 1.0, 40.0 \text{ fm}\}$, which are precise enough for the present purpose. The expansion (2.14) converges quickly with increasing ν , and $\nu \lesssim 100$ ($E_{J\nu} \lesssim 1 \text{ MeV}$ above the $(\alpha X^-) - d$ threshold) is very sufficient. Basis sets for $J \geq 1$ are not shown since contribution to the cross section from $J \geq 1$ is 3 orders of magnitude smaller than that from $J = 0$.

ii) *Basis set for $\alpha + t$ (${}^3\text{He}$) + X^-*

Since $l_2 = 1$ in the exit channel of (2.4) and (2.5), the basis $[\phi_{n_c l_c}^G(\mathbf{r}_c) \psi_{N_c L_c}^G(\mathbf{R}_c)]_{JM}$ for $J = 1$ with $\{(l_1 = 0, L_1 = 1), (l_2 = 1, L_2 = 0)\}$ is of the most important (see Figs. 3 and 4). The next important set for $J = 1$ is $\{(l_1 = 1, L_1 = 0), (l_2 = 1, L_2 = 0)\}$. We take Gaussian ranges $\{r_1, r_{n_{\max}}, R_1, R_{N_{\max}}\} = \{0.4, 15.0, 0.8, 30.0 \text{ fm}\}$ with $n_{\max} = N_{\max} = 12$. Contribution of $J = 0$ to the S -factor is several times smaller than that of $J = 1$; we take the set ($l_c = L_c = 0, 1$) for $c = 1 - 3$.

2.5. Result for ${}^6\text{Li}$ production

In this subsection we study the ${}^6\text{Li}$ production reaction (2.2) that is the most important CBBN reaction. A three-body calculation of (2.2) was reported in Ref. 5) by Hamaguchi *et al.*, and therefore we simply recapitulate it here. The calculated astrophysical S -factor $S(E)$ is shown in Fig. 2 together with the Gamow peak at $E_0 = 33 \text{ keV}$ for $T_9 = 0.1$ ($kT = 8.62 \text{ keV}$) around which (αX^-) is formed. Contribution from the s -wave incoming channel with $(l_1 = L_1 = 0) \rightarrow (l_2 = L_2 = 0)$ is dominant and that from the p -wave one with $(l_1 = 0, L_1 = 1) \rightarrow (l_2 = 0, L_2 = 1)$ is 3 orders of magnitude smaller. A significant effect of the closed-channel amplitude $\Psi_{JM}^{(\text{closed})}$ in (2.12) which stands for the contribution of the three-body degree of freedom in the interaction region is seen as following: If the term $\Psi_{JM}^{(\text{closed})}$ is omitted in the three-body calculation, $S(E)$ becomes nearly 3 times smaller than that in Fig. 2.

The CBBN S -factor in Fig. 2 is enhanced roughly by a factor of $\sim 10^7$ compared with that of the SBBN reaction (2.1). This confirms the large enhancement ($\sim 10^8$) pointed out by Pospelov¹⁾ though his scaling relation for the estimation is too naive. It is to be noted that the S -factor in Fig. 2 is within similar magnitudes of typical non-resonant photonless SBBN reactions and that the large enhancement ratio comes simply from the fact that the SBBN reaction (2.1) is heavily E1-hindered.

The energy-dependence of $S(E)$ in Fig. 2 is approximated by (2.27) with $S(0) = 44.6 \text{ keV b}$ and $\alpha = -0.18 \text{ b}$. The reaction rate is then given, using (2.28), as^{*)}

$$N_A \langle \sigma v \rangle = 2.78 \times 10^8 T_9^{-\frac{2}{3}} \exp(-5.33 T_9^{-\frac{1}{3}}) (1 - 0.62 T_9^{\frac{2}{3}} - 0.29 T_9) \text{ cm}^3 \text{ s}^{-1} \text{ mol}^{-1} \quad (2.36)$$

^{*)} The expression (2.36) is slightly different from (4.3) of Ref. 5). The latter is for the vicinity of $kT = 10 \text{ keV}$ ($T_9 = 0.116$) while the former is available to wider range of $T_9 \lesssim 0.2$.

for $T_9 \lesssim 0.2$. On the other hand, since the SBBN reaction rate of (2.1) is given¹⁷⁾ as

$$N_A \langle \sigma v \rangle_{\text{SBBN}} = 14.8 T_9^{-\frac{2}{3}} \exp(-7.44 T_9^{-\frac{1}{3}}) (1 + 6.57 T_9 + \dots) \text{ cm}^3 \text{ s}^{-1} \text{ mol}^{-1}, \quad (2.37)$$

the CBBN/SBBN ratio of the *reaction rates* is $\sim 10^9$ at $T_9 = 0.1$. This increase of the ratio from that of *S-factors* ($\sim 10^7$) is due to the reduction of the CBBN Coulomb barrier seen by the incoming particle (deuteron) in the expression (2.21).

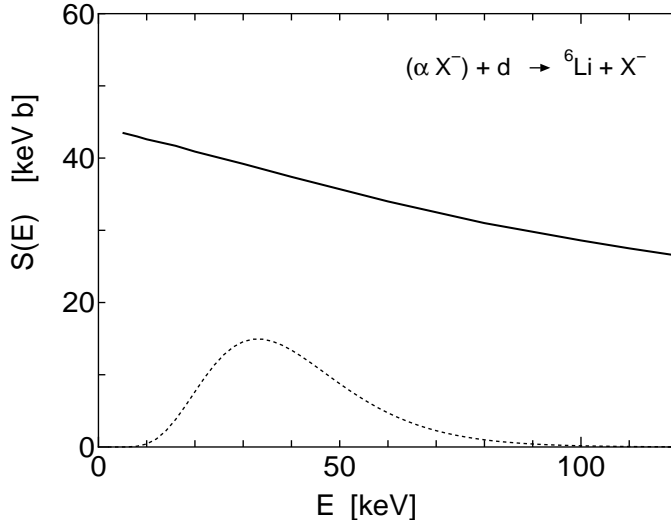


Fig. 2. The astrophysical S -factor of the CBBN reaction (2.2) obtained by the three-body calculation (the solid line). The dotted curve (in arbitrary units) illustrates the Gamow peak for $T_9 = 0.1$ ($kT = 8.62$ keV) with the maximum at $E_0 = 33$ keV. This figure is taken from Ref. 5).

It is desirable to examine quantitatively how sensitive the calculated cross section (S -factor) is to the choice of the $\alpha - d$ potential parameter set that reproduces the empirical $\alpha - d$ binding energy and the measured r.m.s. charge radius of ${}^6\text{Li}$. We did this test by adopting another parameter set $\{r_1 = 0.9$ fm, $V_1 = 400$ MeV, $r_2 = 2.5$ fm, $V_2 = -35.04$ MeV $\}$ which is quite different from the set shown in §2.4. But, we found that the new result of the S -factor differs only by 5 – 6% from that in Fig. 2. One can expect a similar result for other non-resonant reactions studied in the present paper though such a test is not repeated there.

So far, mass of the X^- particle, m_X , is assumed to be 100 GeV. But, we found that the calculated S -factor differs only by ~ 0.5 % between $m_X = 100$ GeV and $m_X \rightarrow \infty$. Therefore, we take $m_X = 100$ GeV throughout the present paper except for §3 where a resonant reaction is studied.

With the use of this large CBBN rate (2.36), Hamaguchi *et al.*⁵⁾ solved the evolution equation for the ${}^6\text{Li}$ abundance after SBBN has frozen out. This calculation was performed for various sets of the assumed lifetime τ_X and the initial number density n_{X^-} of the X^- particle together with calculating the the number of the bound state (αX^-) as a function of the temperature (cf. Fig. 5 of Ref. 5)). For the limiting case of long lifetime ($\tau_X \gg 1000$ s), they obtained $n_{6\text{Li}}/n_B \simeq 3.7 \times 10^{-5} n_{X^-}/n_B$

where $n_{e\text{Li}}$ and n_{B} are the number densities of ${}^6\text{Li}$ and baryons, respectively. Therefore, the observational upper bound on the ${}^6\text{Li}$ abundance ${}^6\text{Li} < 6.1 \times 10^{-11}$ (2σ)³²⁾ leads to a remarkable bound on the X^- abundance, $n_{X^-}/n_{\text{B}} < 1.6 \times 10^{-6}$. Particle physics implication of this result is discussed in Ref. 5).

2.6. Result for ${}^7\text{Li}$ and ${}^7\text{Be}$ production

Calculated astrophysical S -factor of the ${}^7\text{Li}$ -production reaction (2.4) is shown in Fig. 3. Magnitude of $S(E_0)$ at the Gamow-peak energy is approximately one order smaller than that of the ${}^6\text{Li}$ -production reaction in Fig. 2. This is because the ground state of ${}^6\text{Li}$ has s -wave ($l_2 = 0$) angular momentum of the $d-\alpha$ configuration whereas that of ${}^7\text{Li}$ has p -wave ($l_2 = 1$) one between t and α . The incident wave with $l_1 = L_1 = 0$ has to make the angular-momentum rearrangement to $l_2 = L_2 = 1$ in the exit channel, and therefore the most effective partial wave is the one having

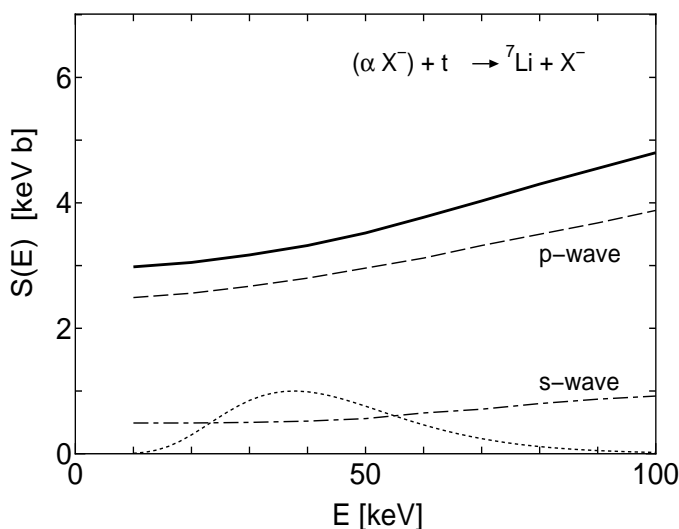


Fig. 3. The S -factor of the CBBN reaction (2.4) obtained by the three-body calculation (the solid line). The s - and p -wave contributions are shown individually. The dotted curve (in arbitrary units) illustrates the Gamow peak for $T_9 = 0.1$ ($kT = 8.6$ keV) with $E_0 = 38$ keV.

$l_1 = 0, L_1 = 1$ in the incident channel and $l_2 = 1, L_2 = 0$ in the exit channel. This is seen in Fig. 3; the contribution of the p -wave ($L_1 = 1$) in the incident channel is much larger than that of the s -wave ($L_1 = 0$).

A large effect of the closed-channel amplitude $\Psi_{JM}^{(\text{closed})}$ in (2.12) which stands for the contribution of the three-body degree of freedom in the interaction region is seen as following: If the term $\Psi_{JM}^{(\text{closed})}$ is omitted in the three-body calculation, $S(E)$ becomes nearly 50 times smaller than that in Fig. 3. The effect changes largely from the case of the ${}^6\text{Li}$ production in §2.5 (namely, from 3 times to 50 times) is due to the fact that the angular-momentum transfer between the entrance and exit channels is rather hard at the low energies much below the Coulomb barrier and therefore the transfer is strongly mediated by the degree of the three-body distortion in the internal region where the reaction takes place.

In the above calculation, the spin of t is neglected and therefore the $3/2^-$ ground state and the $1/2^-$ excited one are degenerated. But, this assumption was found to work well in a further precise calculation with the spin of t and the spin-dependent α - t interaction taken into account explicitly. Namely, the S -factors of the transition to the ground and excited states are found to be respectively 53% and 50% of the S -factor by the present spin-neglected calculation (the solid curve in Fig. 3) in the Gamow-peak region, and therefore their sum (103%) deviates only by 3% from the spin-neglected case although the above percentage numbers deviate respectively from 67% and 33% (proportional to the spin weights) in the case where the $3/2^-$ ground and $1/2^-$ excited states are assumed to have the same degenerated binding energy and the same radial wave function.

The magnitude of $S(E)$ for the ${}^7\text{Li}$ production in CBBN is approximately 30 times larger than the S -factor of the E1 radiative-capture SBBN reaction (2.6) in the Gamow-peak region in Fig. 3, $S_\gamma(E_0) \sim 0.1 \text{ keV b.}^{17)}$ This CBBN/SBBN-enhancement factor of ~ 30 is very much smaller than $\sim 10^7$ in that for the ${}^6\text{Li}$ production. This is simply because the E1 transition in SBBN is allowed in the ${}^7\text{Li}$ production but is heavily hindered in the ${}^6\text{Li}$ production, as was pointed out in §2.1.2. Cyburt *et al.*,⁴⁾ however, predicted a very large CBBN/SBBN-enhancement factor ($\sim 10^5$) assuming the scaling relation.¹⁾ This large overestimation is because the scaling relation which compares the wavelengths of the real and virtual photons is not suited at all for this type of transfer reactions caused by the strong nuclear interaction. On the other hand, Kusakabe *et al.* assumed, in their BBN network calculation,¹²⁾ that the above CBBN processes to create ${}^7\text{Li}$ and ${}^7\text{Be}$ are negligible, taking the same consideration as above on the angular-momentum rearrangement ($l_1 = L_1 = 0$) \rightarrow ($l_2 = L_2 = 1$). Though consideration on the largest contribution from ($l_1 = 0, L_1 = 1$) \rightarrow ($l_2 = 1, L_2 = 0$) is missing in Ref. 12), we support their assumption as a reasonable one. But, our reaction rates given below are to be employed in the BBN network calculation when a precise discussion is made about the abundances of ${}^7\text{Li}$ and ${}^7\text{Be}$.

The energy-dependence of $S(E)$ in Fig. 4 may be approximated by the expression (2.27) with $S(0) = 2.6 \text{ keV b}$ and $\alpha = 0.02 \text{ b}$, and therefore the reaction rate is written, for $T_9 \lesssim 0.2$, as

$$N_A \langle \sigma v \rangle = 1.4 \times 10^7 T_9^{-\frac{2}{3}} \exp(-6.08 T_9^{-\frac{1}{3}}) (1 + 1.3 T_9^{\frac{2}{3}} + 0.55 T_9) \text{ cm}^3 \text{ s}^{-1} \text{ mol}^{-1}. \quad (2.38)$$

As for the ${}^7\text{Be}$ -production reaction (2.5), calculated S -factor is shown in Fig. 4. Almost the same discussions as above on the ${}^7\text{Li}$ production can be made. The S -factor $S(E)$ in Fig. 4 may be approximated with $S(0) = 13.7 \text{ keV b}$ and $\alpha = 0.01 \text{ b}$, and then the reaction rate is written, for $T_9 \lesssim 0.2$, as

$$N_A \langle \sigma v \rangle = 9.4 \times 10^7 T_9^{-\frac{2}{3}} \exp(-9.66 T_9^{-\frac{1}{3}}) (1 + 0.20 T_9^{\frac{2}{3}} + 0.05 T_9) \text{ cm}^3 \text{ s}^{-1} \text{ mol}^{-1}. \quad (2.39)$$

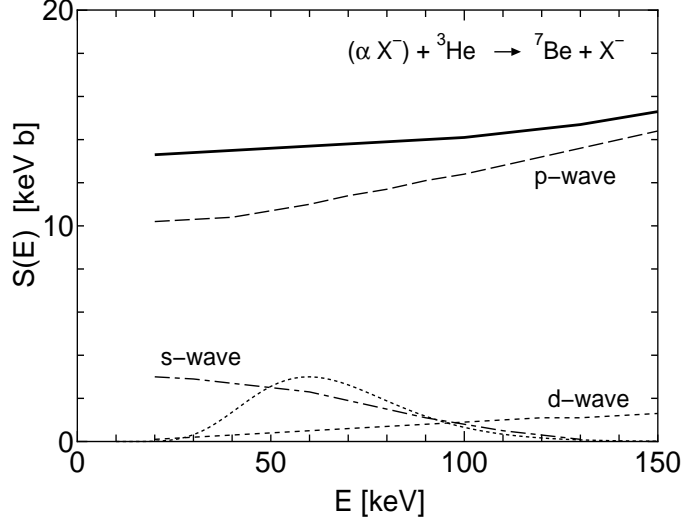


Fig. 4. The S -factor of the CBBN reaction (2.5) obtained by the three-body calculation (the solid line). The s -, p - and d -wave contributions are shown individually. The dotted curve (in arbitrary units) illustrates the Gamow peak for $T_0 = 0.1$ ($kT = 8.6$ keV) with $E_0 = 60$ keV.

§3. X^- -catalyzed radiative capture reactions

3.1. Necessity of three-body calculation

Since the $A = 7$ nuclei are produced dominantly as ${}^7\text{Be}$ (eventually decaying to ${}^7\text{Li}$ by electron capture) in the BBN network calculation with the CMB-based $\eta_{\text{B}} = 6.0 \times 10^{-10}$, any reaction^{*)} to destroy ${}^7\text{Be}$ might be effective to reduce the ${}^7\text{Li}$ -overproduction. For this purpose, Bird *et al.*⁶⁾ considered a resonant radiative capture reaction, (cf. Fig. 5)



where the intermediate state denoted as $({}^8\text{B}X^-)_{2p}^{(\text{res.})}$ is a Feshbach resonance generated by the coupling of the atomic $2p$ excited state, say $({}^8\text{B}X^-)_{2p}$, with the $({}^7\text{Be}X^-) + p$ continuum. Here, we note that after a rapid β -decay, the bound state $({}^8\text{B}X^-)$ transforms to $({}^8\text{Be}(2^+, 3 \text{ MeV})X^-)$ which immediately decays^{**)} to the scattering channel $\alpha + \alpha + X^- + 1.5 \text{ MeV}$.

Assuming a simple Gaussian shape of the charge distribution of the ${}^8\text{B}$ nucleus, Bird *et al.* calculated the energy of $({}^8\text{B}X^-)_{2p}$, E_{2p} , with respect to the ${}^8\text{B} + X^-$ threshold. They obtained $E_{2p} = -1.026 \text{ MeV}$ and estimated the resonance energy, $E_{\text{res.}}$, with respect to the $({}^7\text{Be}X^-) + p$ threshold as $E_{\text{res.}} = E_{2p} + E_{\text{sB}} - E({}^7\text{Be}X^-) =$

^{*)} The reaction $({}^7\text{Be}X^-) + p \rightarrow {}^8\text{B} + X^-$ is energetically impossible due to the negative Q -value (-1.323 MeV); note that binding energy of ${}^8\text{B}$ is only 0.138 MeV .

^{**)} The authors of Refs. 6), 14) erroneously consider that $({}^8\text{B}X^-)$ transforms to $({}^8\text{Be}(\text{g.s.})X^-)$ and that the latter state could potentially lead to a new primordial source of ${}^9\text{Be}$ via $({}^8\text{Be}X^-) + n \rightarrow {}^9\text{Be} + X^-$. Note that ${}^8\text{B}$ shows no β -decay to ${}^8\text{Be}(\text{g.s.})$.

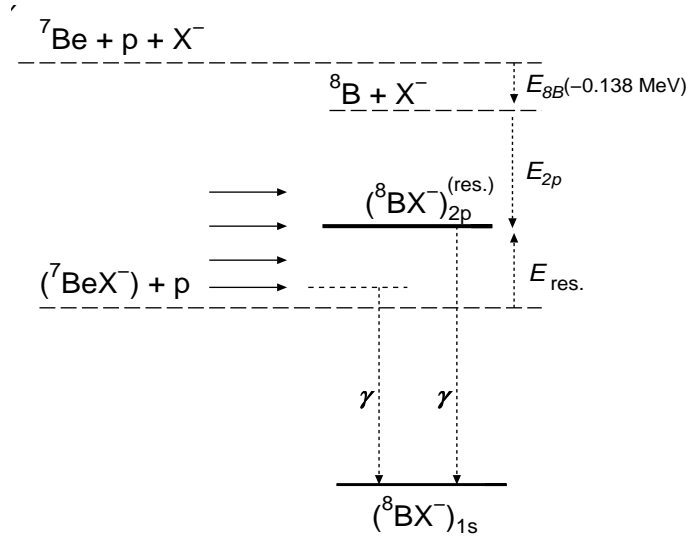
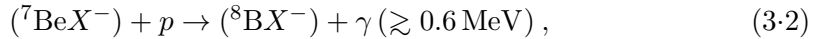


Fig. 5. Schematic illustration of the X^- -catalyzed resonant and non-resonant radiative capture processes (3-1) and (3-2).

0.167 MeV *without* the scattering calculation. Further assuming that the resonance width $\Gamma_{\text{res.}}$ is much larger than the radiative width for decaying to $({}^8\text{B}X^-)_{1s}$, they derived the reaction rate of (3-1) and claimed that the resonant reaction (3-1) is quite effective in reducing the ${}^7\text{Li}$ - ${}^7\text{Be}$ abundance in their BBN network calculation⁶⁾ and in restricting the lifetime and the primordial abundance of the X^- particle.

As is discussed below, the rate of the resonant reaction depends strongly on $E_{\text{res.}}$, but the model of Ref. 6) is too simple to treat the resonance state. Therefore, in this section, we perform a precise ${}^7\text{Be} + p + X^-$ three-body scattering calculation of the resonant reaction (3-1) as well as the non-resonant radiative capture reaction



though the reaction rate of (3-2) is much smaller than that of (3-1).

Since the rate of the resonant reaction is proportional to $\exp(-E_{\text{res.}}/kT)$, a small change in $E_{\text{res.}}$ can generate a large change in the rate; for example, at $T_9 = 0.3$ ($kT = 25 \text{ keV}$), increase (decrease) of 50 keV in $E_{\text{res.}}$ changes the reaction rate by a factor of $e^2 (= 7.4)$. The 50-keV change is only 5% of the binding energy ($-E_{2p} \sim 1.0 \text{ MeV}$) of the $({}^8\text{B}X^-)_{2p}$ state, and therefore it is absolutely required to calculate $E_{\text{res.}}$ with the structure of the ${}^8\text{B}$ nucleus taken into account in details.

Since the nucleus ${}^8\text{B}$ has extensively been studied mainly from the viewpoint of physics of unstable nuclei and that of the solar neutrino problem, information about ${}^8\text{B}$ has been much accumulated.³³⁾⁻³⁹⁾ The ground state of ${}^8\text{B}$, being very weakly bound ($E_{s\text{B}} = -0.138 \text{ MeV}$) with respect to the ${}^7\text{Be} + p$ threshold, is known to have a p -wave proton *halo* (a long-range tail) of the ${}^7\text{Be} + p$ structure. Therefore, as will be shown below, the charge distribution of ${}^8\text{B}$ has a long-range *quadrupole* component which generates the anisotropic part of the Coulomb potential between ${}^8\text{Be}$ and X^- . The expectation value of this part by the $({}^8\text{B}X^-)_{2p}$ wave function

amounts to some -50 keV ($J = 0$), $+10$ keV ($J = 1$) and $+30$ keV ($J = 2$) where J denotes the total angular momentum to which the p -wave ${}^7\text{Be} - p$ relative motion in ${}^8\text{B}$ and the p -wave relative motion between ${}^8\text{B}$ and X^- couples (see (3.3) below).

Another important factor that we have to consider concerning ${}^8\text{B}$ is spins of the ${}^7\text{Be}$ ($3/2^-$) core and the valence proton ($1/2$). The two spins couple with the p -wave angular momentum between ${}^7\text{Be}$ and p to the total angular momentum 2^+ in the ground state. The other possible spin-coupling states are not bound; excitation energies of the 1^+ and 3^+ resonance states are 0.77 MeV and 2.32 MeV. Therefore, we cannot neglect the fact that the ground state of ${}^8\text{B}$ has the specific spin 2^+ .

However, estimation of E_{2p} in Ref. 6) was made assuming an isotropic Gaussian form of the charge distribution of ${}^8\text{B}$ with neither ${}^7\text{Be} + p$ structure nor spins of the particles taken into account. In this section, we investigate the reactions (3.1) and (3.2) adopting explicitly the ${}^7\text{Be} + p + X^-$ three-body degree of freedom by which the very diffuse, anisotropic charge distribution of ${}^8\text{B}$ ($= {}^7\text{Be} + p$) is automatically taken into account. Use of this three-body model makes it possible to calculate not only the precise resonance energy E_{res} , but also the cross section of the first transition process in (3.1) that could not be treated by the model of structureless ${}^8\text{B}$ in Ref. 6).

3.2. Resonance energy by approximate models of ${}^8\text{B}$

Before making the three-body calculation, we employ four types of approximate models of ${}^8\text{B}$, *Models* i) to iv) below, and discuss about how the energy of the $({}^8\text{B}X^-)_{2p}$ state, E_{2p} , depends on the assumed structure of ${}^8\text{B}$ though we do not couple the state to the ${}^7\text{Be} + p$ scattering state. This may be an instructive guide to the sophisticated three-body scattering calculation in §3.3 and §3.4.

Model i) Bird *et al.*⁶⁾ assumed a Gaussian shape of the charge distribution of ${}^8\text{B}$ with the r.m.s. charge radius 2.64 fm. This gives $E_{2p} = -1.026$ MeV ($m_X \rightarrow \infty$ is taken throughout this subsection) which corresponds to the resonance energy $E_{\text{res}}^{(i)} = 167$ keV above the $({}^7\text{Be}X^-) + p$ threshold at -1.330 MeV with respect to the ${}^7\text{Be} + X^- + p$ three-body breakup threshold (see Fig. 5). But, this assumption of the Gaussian-shape charge density is not appropriate for this special nucleus ${}^8\text{B}$.

Model ii) The ${}^8\text{B}$ nucleus is known to have a very-loosely bound ${}^7\text{Be} + p$ structure with a p -wave proton halo around the ${}^7\text{Be}$ core.³⁵⁾⁻³⁸⁾ Neglecting spins of ${}^7\text{Be}$ ($3/2^-$) and the valence proton ($1/2^-$), we firstly calculate the p -state ${}^7\text{Be} - p$ wave function using the most popularly known ${}^7\text{Be} - p$ potential³⁸⁾ (parameters are given in §3.3). By assuming the charge density of ${}^7\text{Be}$ (proton) to have the Gaussian shape with the observed r.m.s. charge radius 2.52 fm³³⁾ (0.8750 fm³⁰⁾), we calculate the charge density of the ground state of ${}^8\text{B}$. Due to the p -state wave function, the density has both an isotropic monopole part and a deformed quadrupole part. The former is illustrated in Fig. 6 together with the contributions from ${}^7\text{Be}$ and p . The density significantly deviates from the Gaussian shape in the tail region due to the proton halo. If we take the ${}^8\text{B} - X^-$ Coulomb potential due to the monopole charge density alone, we have $E^{(\text{mono})}(2p) = -1.009$ MeV which corresponds to $E_{\text{res}}^{(ii)} = 184$ keV. This increase of E_{res} , by 17 keV compared with 167 keV in *Model* i), *reduces* the reaction rate of (3.1) by a factor of 2 at $T_9 = 0.3$.

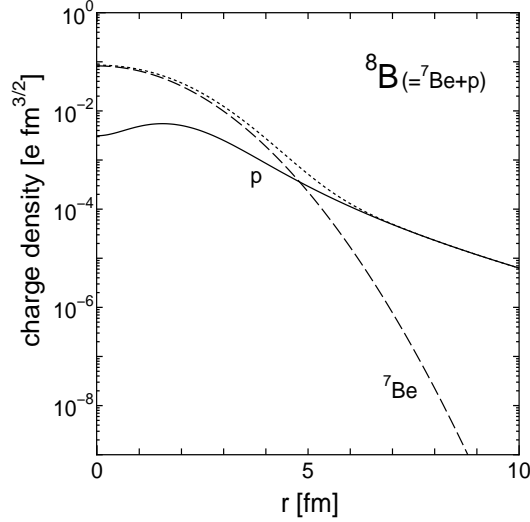


Fig. 6. Monopole part of the charge density, $\rho(r)$, of ${}^8\text{B}$ (dotted line) calculated with the ${}^7\text{Be} + p$ model. The solid (dashed) line shows the contribution from the proton (${}^7\text{Be}$). $\rho(r)$ is normalized as $\int \rho(r) dr = 5$, r being the distance measured from the c.m. of ${}^8\text{B}$.

Model iii) Taking above *Model ii)*, we further consider the contribution from the quadrupole part of the charge density of ${}^8\text{B}$. Let $\phi_{1m}(\mathbf{r}_2)$ and $\psi_{1M}(\mathbf{R}_2)$ denote the wave functions of the p -wave ${}^8\text{B}$ ground state and that of the atomic $2p$ relative motion between ${}^8\text{B}$ and X^- which have already been obtained in ii). Then,

$$\Psi_{JM}^{(\text{iii})} = [\phi_1(\mathbf{r}_2) \otimes \psi_1(\mathbf{R}_2)]_{JM} \quad (J = 0, 1, 2) \quad (3.3)$$

is the total wave function of the $({}^8\text{B}X^-)_{2p}$ state^{*} having the angular momentum J and its z -component M . The quadrupole part of the Coulomb potential between ${}^8\text{B}$ and X^- , which is sensitive to the angle between \mathbf{r}_2 and \mathbf{R}_2 , should contribute to the total energy dependently on the angular momentum coupling to J . The expectation value of Hamiltonian with respect to $\Psi_{JM}^{(\text{iii})}$, say $E_J^{(\text{iii})}(2p)$, is written as

$$E_J^{(\text{iii})}(2p) = E^{(\text{mono})}(2p) + \Delta E_J^{(\text{quad})}(2p), \quad (3.4)$$

where $\Delta E_J^{(\text{quad})}(2p)$ is the contribution from the quadrupole part of the charge density of ${}^8\text{B}$ mentioned above and $E^{(\text{mono})}(2p)$ was given in *Model ii)*. We obtain $\Delta E_J^{(\text{quad})}(2p) = -54 \text{ keV}$ ($J = 0$), $+27 \text{ keV}$ ($J = 1$) and -5.4 keV ($J = 2$), and therefore, $E_J^{(\text{iii})}(2p) = -1.063 \text{ keV}$ ($J = 0$), -1.036 keV ($J = 1$) and -1.014 keV ($J = 2$), which correspond to $E_{\text{res.}}^{(\text{iii})} = 130 \text{ keV}$ ($J = 0$), 211 keV ($J = 1$) and 179 keV ($J = 2$). In the case of $J = 0$, the resonance energy $E_{\text{res.}} = 130 \text{ MeV}$ results in a reaction rate that is 8 times larger than that of *Model ii)*. But, we should not stop here since we have not included yet the effect of spins of ${}^7\text{Be}$ ($3/2^-$), p ($1/2$) and ${}^8\text{B}$ (2^+).

^{*} In this notation of $({}^8\text{B}X^-)_{2p}$ in *Model iii)*, the p -wave angular momentum of ${}^8\text{B}$ and the total angular momentum J are not explicitly written for simplicity, and similarly in *Model iv)*.

Model iv) Spin-parity of the ground state of ${}^8\text{B}$ is 2^+ . In the literature papers on ${}^8\text{B}$ taking the ${}^7\text{Be} + p$ model, structure of low-lying states of ${}^8\text{B}$ is considered as following: the valence proton is located in the $p_{3/2}$ orbit around the ${}^7\text{Be}$ ($3/2^-$) core, and the two $3/2^-$ spins are coupled to the total angular momentum $I = 2^+$ in the ground state and $I = 1^+$ and 3^+ in the excited states with the observed $E_x = 0.77$ MeV and 2.32 MeV, respectively. Since the spin dependent interaction is so strong and the Coulomb interaction between ${}^8\text{B}$ and X^- does not change the spin structure, we have to consider seriously the ground-state spin 2^+ and its coupling scheme in the calculation of the resonance energy. Let $\phi_{\{p_{3/2}, 3/2\}IM_I}(\mathbf{r}_2)$ denote the wave function of the ground state ($I = 2$) of ${}^8\text{B}$ explained above. The total wave function of the $({}^8\text{B}X^-)_{2p}$ state is written as

$$\Psi_{JM}^{(\text{iv})} = \left[\phi_{\{p_{3/2}, 3/2\}I}(\mathbf{r}_2) \otimes \psi_1(\mathbf{R}_2) \right]_{JM}, \quad (3.5)$$

where $\psi_1(\mathbf{R}_2)$ was given in *Model ii*). The expectation value of the Hamiltonian with respect to $\Psi_{JM}^{(\text{iv})}$, say $E_{J,I}^{(\text{iv})}(2p)$, is described in the form

$$E_{J,I}^{(\text{iv})}(2p) = E^{(\text{mono})}(2p) + \sum_{\Lambda=0}^2 a_{J,I\Lambda} \Delta E_{\Lambda}^{(\text{quad})}(2p) \quad (3.6)$$

where $E^{(\text{mono})}(2p)$ and $\Delta E_{\Lambda}^{(\text{quad})}(2p)$ are given in (3.4), and $a_{J,I\Lambda}$ is written as

$$a_{J,I\Lambda} = \frac{1}{2}(2J+1)(2\Lambda+1) \sum_{S=1}^2 [W(1I\Lambda J; S1)]^2. \quad (3.7)$$

The second term of Eq.(3.6) accidentally vanishes due to the summation over S for the ground-state spin $I = 2$ but not for $I \neq 2$. We then have $E_{J,I}^{(\text{iv})}(2p) = E^{(\text{mono})}(2p) = -1.009$ MeV for $I = 2^+$, and therefore $E_{\text{res.}}^{(\text{iv})} = 184$ MeV ($J = 1, 2$) which is, by chance, the same as in *Model ii*).

3.3. Three-body calculation of resonance energy and width

In the four-types of approximate models of $({}^8\text{B}X^-)_{2p}$ in the previous subsection, ${}^8\text{B}$ is assumed to be the same as that in the free space. But, since ${}^8\text{B}$ is a very loosely bound state of ${}^7\text{Be}$ and p , it is possible that the spatial structure of ${}^8\text{B}$ changes in the presence of X^- , namely in the presence of the Coulomb potential between ${}^7\text{Be}$ and X^- and that between p and X^- (the spin structure is not changed by those Coulomb potentials). Therefore, using the ${}^7\text{Be} + p + X^-$ three-body model with the Hamiltonian (2.9), we calculate the resonance state as a Feshbach resonance embedded in the $({}^7\text{Be}X^-) + p$ continuum and precisely determine the energy and width of the resonance.

3.3.1. Nuclear and Coulomb potentials

Following the literature ${}^7\text{Be} + p$ model we treat ${}^7\text{Be}$ as an inert core with spin $3/2^-$. We assume Gaussian-shape charge distributions of ${}^7\text{Be}$ and the proton as $4e(\pi b_{\text{Be}}^2)^{-3/2} e^{-(r/b_{\text{Be}})^2}$ and $e(\pi b_p^2)^{-3/2} e^{-(r/b_p)^2}$, respectively, and take $b_{\text{Be}} = 2.06$ fm

and $b_p = 0.714$ fm in order to reproduce the observed r.m.s. charge radii, 2.52 fm³³⁾ for ${}^7\text{Be}$ and 0.8750 fm³⁰⁾ for the proton. The Coulomb potential between ${}^7\text{Be}$ and X^- is then given by

$$V_{{}^7\text{Be}-X}(r) = -4e^2 \frac{\text{erf}(r/b_{\text{Be}})}{r}, \quad (3.8)$$

and that between X^- and p is written as

$$V_{p-X}(r) = -e^2 \frac{\text{erf}(r/b_p)}{r}. \quad (3.9)$$

Energy of $({}^7\text{Be}X^-)_{1s}$ is $\varepsilon_{\text{g.s.}}^{(1)} = -1.386$ (-1.324) MeV and the r.m.s. radius is 3.60 (3.49) fm for $m_X = 100$ GeV ($m_X \rightarrow \infty$).

The potential $V_{{}^7\text{Be}-p}(r)$ is a sum of the nuclear potential, $V_{{}^7\text{Be}-p}^{\text{N}}(r)$, and the Coulomb potential, $V_{{}^7\text{Be}-p}^{\text{C}}(r)$. The latter is given by

$$V_{{}^7\text{Be}-p}^{\text{C}}(r) = 4e^2 \frac{\text{erf}(r/\sqrt{b_{\text{Be}}^2 + b_p^2})}{r}. \quad (3.10)$$

As for the nuclear potential $V_{{}^7\text{Be}-p}^{\text{N}}(r)$ between ${}^7\text{Be}$ and p , we follow the work of Ref. 38) that is a standard study of the ${}^7\text{Be} + p \rightarrow {}^8\text{B} + \gamma$ reaction. The nuclear potential is parameterized as a Woods-Saxon plus a spin-orbit potential with an adjustable depth $V_0(lj, I)$:

$$V_{{}^7\text{Be}-p}^{\text{N}}(r) = \left[1 - F_{\text{s.o.}}(\mathbf{l} \cdot \mathbf{s}) \frac{r_0}{r} \frac{d}{dr} \right] \frac{V_0(lj, I)}{1 + \exp[(r - R_0)/a]}. \quad (3.11)$$

Here, we take $a = 0.52$ fm, $R_0 = 2.391$ fm and $F_{\text{s.o.}} = 0.351$ fm.³⁸⁾ The orbital and total angular momenta of the proton are denoted by (lj) . The $I = 2^+$ ground state of ${}^8\text{B}$ is described in terms of a pure $(lj) = p_{3/2}$ orbit of the proton coupled with spin $3/2^-$ of the ${}^7\text{Be}$ core. The well depth $V_0(l = 1, j = 3/2, I = 2)$ is adjusted to reproduce the binding energy of 0.1375 MeV of the ground state and is given by -44.147 MeV. The s -wave potential between ${}^7\text{Be}$ and p is assumed to have $V_0 = -30.0$ MeV, $R_0 = 2.39$ fm, $a = 0.65$ fm and have additionally a Pauli repulsive potential with $V_0 = 800$ MeV, $R_0 = 1.5$ fm, $a = 0.2$ fm. This s -wave potential gives no bound state.

3.3.2. Resonance wave function

Let $\xi_{\frac{3}{2}}({}^7\text{Be})$ and $\xi_{\frac{1}{2}}(p)$ denote the spin functions of the ${}^7\text{Be}$ ground state and the proton, respectively. The $1s$ ground state of $({}^7\text{Be}X^-)$ is described by $\phi_{00}^{(1)}(\mathbf{r}_1)$. We consider the s -state relative wave function between the incident proton and the target $({}^7\text{Be}X^-)$, say $\chi_{00}^{(1)}(\mathbf{R}_1) (= \chi_0^{(1)}(R_1)Y_{00}(\hat{\mathbf{R}}_1))$, since the p -state one has the different parity and the d -state one has negligible coupling to the contribution to the resonant radiative capture process. There is neither inelastically excited channels in $c = 1$ nor transfer channels in $c = 2, 3$ for the energies (< 200 keV) concerned here. The total wave function to describe the resonant state is then written as

$$\Psi_{JM} = \phi_{00}^{(1)}(\mathbf{r}_1) \chi_{00}^{(1)}(\mathbf{R}_1) \left[\xi_{\frac{3}{2}}({}^7\text{Be}) \otimes \xi_{\frac{1}{2}}(p) \right]_{JM} + \Psi_{JM}^{(\text{closed})}. \quad (3.12)$$

The second term of (3.12), $\Psi_{JM}^{(\text{closed})}$, stands for the internal amplitude of the resonance wave function whose approximate expression is $\Psi_{JM}^{(\text{iv})}$ of (3.5). But, we here describe $\Psi_{JM}^{(\text{closed})}$ taking the three-body degrees of freedom in the same way as in §2.4. Since we find that, in (3.12), contributions from the amplitudes with $c = 1$ and 3 are negligible in the resonance energy region, we here express $\Psi_{JM}^{(\text{closed})}$ as

$$\Psi_{JM}^{(\text{closed})} = \sum_{\nu=1}^{\nu_{\text{max}}} b_{J\nu} \Phi_{JM,\nu}^{(2)} \quad (3.13)$$

using the three-body basis functions only in $c = 2$ together with the spin functions,

$$\Phi_{JM,\nu}^{(2)} = \sum_{n_2, N_2} A_{J\nu, n_2, N_2}^{(2)} \left[[[\phi_{n_2 l_2}^G(\mathbf{r}_2) \otimes \xi_{\frac{1}{2}}(p)]_{\frac{3}{2}} \otimes \xi_{\frac{3}{2}}(^7\text{Be})]_I \otimes \psi_{N_2 L_2}^G(\mathbf{R}_2) \right]_{JM}, \quad (3.14)$$

where $l_2 = L_2 = 1, I = 2$ and $J = 1, 2$ are sufficient for the resonant reaction. As for the Gaussian ranges in (2.34) and (2.35), we take $n_{\text{max}} = N_{\text{max}} = 15$ ($\nu_{\text{max}} = 225$) and $\{r_1, r_{n_{\text{max}}}, R_1, R_{N_{\text{max}}}\} = \{0.4, 15.0, 0.6, 20 \text{ fm}\}$, which is sufficiently precise for the present purpose.

By diagonalizing the three-body Hamiltonian, we obtain eigenstates $\{\Phi_{JM,\nu}; \nu = 1 - \nu_{\text{max}}\}$ among which the energy of the lowest-lying state ($\Phi_{JM,\nu=1}$) measured from the $^7\text{Be} + p$ threshold is 198, 186, 177 and 174 keV for $m_X = 50, 100, 500$ GeV and $m_X \rightarrow \infty$, respectively ($J = 1, 2$). The m_X -dependence in the energies comes from the fact that the kinetic energy and the $^7\text{Be} + p$ threshold energy depend on m_X .

The total wave function (3.12) is solved under the scattering boundary condition

$$\lim_{R_1 \rightarrow \infty} R_1 \chi_0^{(1)}(R_1) = u_0^{(-)}(k_1, R_1) - S_{1 \rightarrow 1}^J u_0^{(+)}(k_1, R_1) \quad (3.15)$$

on the basis of the same prescription of §2.2. The resonance state should appear around the energy of the pseudostate $\Phi_{JM,\nu=1}$ mentioned above. The calculated partial-wave elastic scattering cross section is illustrated in Fig. 7 for $J = 1^-$ with $m_X = 50, 100, 500$ GeV and $m_X \rightarrow \infty$; similar behaviour is obtained for the resonance with $J = 2^-$. The energy E_{res}^J and the proton width Γ_p^J of the resonance are summarized in Table I.

3.4. Result for the resonant radiative capture

The final state, ($^8\text{B}X^-$), of the radiative reactions (3.1) and (3.2) is obtained as the ground state of the $^7\text{Be} + p + X^-$ system. The dominant component is obviously the product of the 2^+ ground-state wave function of ^8B and the $1s$ wave function of ($^8\text{B}X^-$). We describe it more precisely using the same three-body basis functions of (3.14) with $l_2 = 1, L_2 = 0, I = 2$ and $J = 2$ with the same ranges of the Gaussian basis. Other configurations are not necessary within the accuracy required in the present purpose. By diagonalizing the three-body Hamiltonian, we obtained the ground-state wave function, $\Phi_{J=2^+M}^{(\text{g.s.})}$ and its energy $E_{\text{g.s.}}$ which is listed in the next last column of Table I.

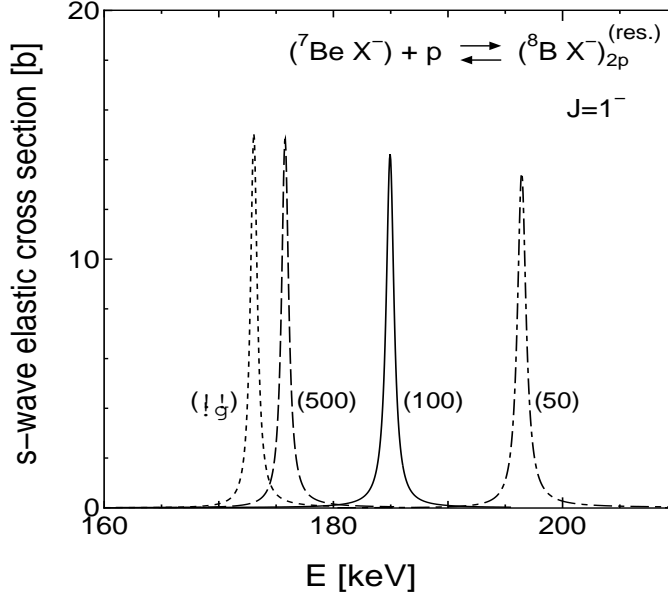


Fig. 7. Partial-wave ($J = 1^-$, s -wave) cross section of the elastic $({}^7\text{Be}X^-)_{1s} + p$ scattering near $({}^7\text{Be}X^-)_{2p}^{\text{res.}}$ for the cases of $m_X = 50$ GeV (dash-dotted line), 100 GeV (solid line), 500 GeV (dashed line) and $m_X \rightarrow \infty$ (short dashed line). Similar behaviour is seen for $J = 2^-$ (s -wave).

The width of the electric dipole (E1) transition from the resonance state $\Psi_{JM}^{(\text{res.})}$ with J^- to the 2^+ ground state is given by

$$\Gamma_\gamma^J = \frac{16\pi k_\gamma^3}{9} \frac{1}{2J+1} \sum_{MM'\mu} |\langle \Phi_{2M'}^{(\text{g.s.})} | Q_{1\mu}^{(E1)} | \Psi_{JM}^{(\text{res.})} \rangle|^2, \quad (J = 1, 2) \quad (3.16)$$

where the E1 operator $Q_{1\mu}^{(E1)}$ is defined by

$$Q_{1\mu}^{(E1)} = \sum_{i=1}^3 q_i R_i^G Y_{1\mu}(\hat{\mathbf{R}}_i^G). \quad (3.17)$$

Here q_i and \mathbf{R}_i^G are the i -th particle's charge and position vector measured from the c.m. of the total system, respectively, and k_γ is the photon wave number. The calculated values of Γ_γ^J are listed in Table I; they are, as expected, close to the width (10.4 eV) given by the simple atomic E1 transition $({}^8\text{B}X^-)_{2p} \rightarrow ({}^8\text{B}X^-)_{1s}$.

Finally, the reaction rate of the resonant radiative capture process is given by using the formula for the reaction (Eq.(4-194) in Ref. 26)) as :

$$N_A \langle \sigma v \rangle = N_A \hbar^2 \left(\frac{2\pi}{M_1 kT} \right)^{\frac{3}{2}} \sum_{J=1}^2 \frac{2J+1}{(2I_1+1)(2I_2+1)} \frac{\Gamma_p^J \Gamma_\gamma^J}{\Gamma_p^J + \Gamma_\gamma^J} \exp\left(-\frac{E_{\text{res.}}^J}{kT}\right), \quad (3.18)$$

where I_1 and I_2 are the spins of ${}^7\text{Be}$ ($3/2$) and p ($1/2$). Here, we consider that the total width of the resonance, $\Gamma_{\text{res.}}$, is given by $\Gamma_p^J + \Gamma_\gamma^J$ since there is no other

Table I. The ${}^7\text{Be} + X^- + p$ three-body calculation of the energy ($E_{\text{res.}}$), the proton-decay width (Γ_p) and the radiative decay width (Γ_γ) of the resonance states with $J = 1^-$ and $J = 2^-$ as well as the energy ($E_{\text{g.s.}}$) of the three-body ground state with $J = 2^+$. $E_{\text{res.}}$ and $E_{\text{g.s.}}$ are measured from the $({}^7\text{Be}X^-)_{1s} + p$ threshold whose energy (E_{th}) is given in the last column with respect to the three-body breakup threshold. All is calculated for $m_X = 50, 100, 500$ GeV and $m_X \rightarrow \infty$.

m_X [GeV]	$J = 1^-$ (res.)			$J = 2^-$ (res.)			$J = 2^+$ (g.s.)	threshold
	$E_{\text{res.}}^J$ [keV]	Γ_p^J [keV]	Γ_γ^J [eV]	$E_{\text{res.}}^J$ [keV]	Γ_p^J [keV]	Γ_γ^J [eV]	$E_{\text{g.s.}}$ [keV]	E_{th} [keV]
50	196.4	0.90	9.1	196.9	0.55	9.1	-624.2	(-1252.0)
100	185.0	0.82	9.6	185.5	0.50	9.6	-635.5	(-1286.1)
500	175.8	0.74	9.9	176.3	0.44	9.9	-643.6	(-1316.4)
∞	173.0	0.71	10.1	173.6	0.43	10.1	-645.9	(-1324.0)

decaying channel. We replace the resonance energies $E_{\text{res.}}^J$ ($J = 1, 2$) by their average, since they are almost the same. We then obtain (in units of $\text{cm}^3 \text{s}^{-1} \text{mol}^{-1}$)

$$N_A \langle \sigma v \rangle = 1.37 \times 10^6 T_9^{-\frac{3}{2}} \exp(-2.28/T_9), \quad (m_X = 50 \text{ GeV}) \quad (3-19)$$

$$N_A \langle \sigma v \rangle = 1.44 \times 10^6 T_9^{-\frac{3}{2}} \exp(-2.15/T_9), \quad (m_X = 100 \text{ GeV}) \quad (3-20)$$

$$N_A \langle \sigma v \rangle = 1.48 \times 10^6 T_9^{-\frac{3}{2}} \exp(-2.04/T_9), \quad (m_X = 500 \text{ GeV}) \quad (3-21)$$

$$N_A \langle \sigma v \rangle = 1.51 \times 10^6 T_9^{-\frac{3}{2}} \exp(-2.01/T_9). \quad (m_X \rightarrow \infty) \quad (3-22)$$

The m_X -dependence of the rates is not negligible since, at $T_9 = 0.3$, their ratios are $0.37 : 0.60 : 0.88 : 1.0$ for $m_X = 50, 100, 500$ GeV and $m_X \rightarrow \infty$. The rate by Bird *et al.* in the second part of Eq.(3-22) in Ref. 6) for $m_X \rightarrow \infty$ is by chance close to our Eq.(3-22); at $T_9 = 0.3$, their rate is 1.2 times of ours, but the models are quite different to each other.

3.5. Result for the non-resonant radiative capture

In this subsection, we investigate the non-resonant (direct) radiative capture process (3-2) using the ${}^7\text{Be} + p + X^-$ three-body model. But, here, we ignore the intrinsic spins of ${}^7\text{Be}$ and p because, as will be shown below, the calculated reaction rate without the spins is 4 orders of magnitude smaller than that of the resonant reaction (3-1). Further inclusion of the spins will not change the result meaningfully.

We consider the non-resonant E1 radiative capture from the $J = 0$ incoming state of the $({}^7\text{Be}X^-) + p$ channel to the $J = 1$ ground state in which the ${}^7\text{Be}$ and p is dominantly in a p -wave relative motion (other partial-wave states are negligible), and denote the wave functions respectively as $\Psi_{00}(E)$ and $\Phi_{1M}^{(\text{g.s.})}$ with the proper normalization. The wave functions can be obtained by using the same methods as in the previous subsections, but the second term of (3-12) can be neglected for the present non-resonant scattering wave.

Cross section of the E1 capture is given by

$$\sigma_{\text{cap.}}^{(E1)}(E) = \frac{16\pi}{9} \frac{k_\gamma^3}{\hbar v_1} \sum_M |\langle \Phi_{1M}^{(\text{g.s.})} | Q_{1M}^{(E1)} | \Psi_{00}(E) \rangle|^2, \quad (3.23)$$

where k_γ is the wave number of the emitted photon and v_1 is the velocity of the relative motion between (${}^7\text{Be}X^-$) and p .

Calculated $S(E)$ of the CBBN reaction (3.2) is illustrated in Fig. 8 in the Gamow-peak region together with the observed S -factor¹⁷⁾ of the SBBN-partner reaction

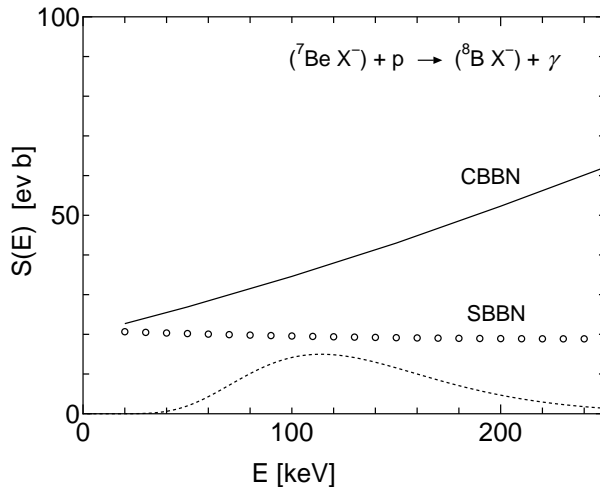


Fig. 8. The astrophysical S -factor (the solid line) of the *non-resonant* radiative-capture CBBN reaction (3.2) obtained by the three-body calculation. The observed S -factor of the SBBN-partner reaction (3.24) is shown by the open circles.¹⁷⁾ The dotted curve illustrates the Gamow peak (in arbitrary units) for $T_9 = 0.3$ ($kT = 35$ keV) with the peak maximum at $E_0 = 114$ keV.

The enhancement ratio CBBN/SBBN of the S -factor is only $1 \sim 2$ in the Gamow-peak region for the non-resonant radiative capture processes (3.2) and (3.24). However, in the work of Bird *et al.*,⁶⁾ this ratio is estimated to be so large as ~ 700 . Origin of this enormous overestimation is due to too crude assumption in their model. Namely, they assumed that magnitude of the three-body E1 matrix element in Eq.(3.23) is the same as that of the two-body E1 matrix element in SBBN. This is a wrong assumption because, in the SBBN matrix element, the dominant contribution comes from the very asymptotic tail region of the distance between ${}^7\text{Be}$ and the proton (along \mathbf{r}_2) in the loosely-bound ground state of ${}^8\text{B}$, but, in the CBBN matrix element, the contribution is heavily suppressed due to the presence of X^- as following: (i) in the $({}^7\text{Be}X^-)_{1s}$ state of the initial channel, the distance between ${}^7\text{Be}$ and X^- along \mathbf{r}_1 is short ranged (the r.m.s. radius is ~ 3.5 fm), (ii) in the final state $\Psi_{00}(E)$, the distance between ${}^8\text{B}$ and X^- along \mathbf{R}_2 is also short ranged (the r.m.s. radius is ~ 3 fm) and then (iii) these strongly confine the possible ${}^7\text{Be} - p$ distance

(along $\mathbf{r}_2 = \mathbf{R}_2 - \mathbf{r}_1$) which is effective in the three-body E1 matrix element. Therefore the contribution from the asymptotic region along \mathbf{r}_2 is heavily suppressed. The CBBN/SBBN ratio of the S -factor becomes larger, in the scaling model of Ref. 6), as the binding energy of (${}^8\text{B}X^-$) increases, but, at the same time, the wave function of (${}^8\text{B}X^-$) shrinks and therefore the three-body E1 matrix element becomes smaller. Consideration on this mechanism was missing in the simple model of Ref. 6) for the non-resonant radiative capture reaction.

The fact that the CBBN and SBBN S -factors have similar magnitudes, within nearly factor of 2, in the Gamow-peak region in Fig. 8 suggests an approximate model for the cross section $\sigma_{\text{cap.}}^{(\text{E1})}(E)$ of the CBBN reaction. The cross section may roughly be derived from (2.21) but employing the observed S -factor of the SBBN-reaction and the Coulomb-barrier penetration factor of the CBBN channel. Here, the SBBN-*partner* reaction is defined as the reaction that is given just by removing X^- from a CBBN reaction*). This approximate model will further be examined in the next section for complicated CBBN three-body breakup reactions.

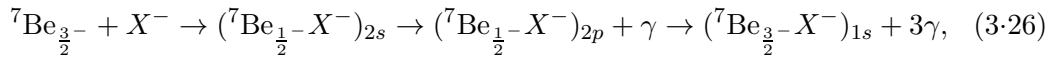
In Fig. 8, since the energy-dependence of $S(E)$ may be approximated by (2.27) with $S(0) = 20 \times 10^{-3}$ keV b and $\alpha = 0.15 \times 10^{-3}$ b, the reaction rate is written as

$$N_A \langle \sigma v \rangle = 2.3 \times 10^5 T_9^{-\frac{2}{3}} \exp(-8.83 T_9^{-\frac{1}{3}}) (1 + 1.9 T_9^{\frac{2}{3}} + 0.54 T_9) \text{ cm}^3 \text{ s}^{-1} \text{ mol}^{-1}, \quad (3.25)$$

for $T_9 \lesssim 0.5$. Since this rate is 4 orders of magnitude smaller than that of the resonant reaction (3.1) at $T_9 = 0.3 - 0.5$, the non-resonant radiative capture reaction (3.2) will play a very minor role in the BBN network calculation.

3.6. Comment on resonant recombination between ${}^7\text{Be}$ and X^-

The radiative capture processes (3.1) and (3.2) are preceded by the recombination of ${}^7\text{Be}$ and X^- to form (${}^7\text{Be}X^-$). Bird *et al.*⁶⁾ calculated the reaction rates of the resonant and non-resonant processes of the recombination. We have a serious comment on a part of their calculation. Besides the normal recombination processes (2.7) and (2.8) in Ref. 6), they specially considered another resonant recombination process (2.12) in Ref. 6),



where ${}^7\text{Be}_{\frac{3}{2}^-}$ and ${}^7\text{Be}_{\frac{1}{2}^-}$ are the ground state and the first excited state at $E_x = 0.429$ MeV, respectively. Their calculation of the energy of the intermediate state (${}^7\text{Be}_{\frac{1}{2}^-} X^-$)_{2s} with $m_X \rightarrow \infty$ gives 49 keV *below* the ${}^7\text{Be}_{\frac{3}{2}^-} + X^-$ threshold, which means that the intermediate state cannot be a resonance in (3.26). Bird *et al.*, however, artificially pushed the state upward to the resonant energy of +10 keV above the threshold and derived a large recombination rate, Eq.(2.13) of Ref. 6). As the reason to do so, they expected ‘a sizable nuclear uncertainty’ such as correction for the finite mass of X^- , a larger charge radius of the excited state, and correction for

*) For instance, the reaction $\alpha + d \rightarrow {}^6\text{Li} + \gamma$ is not the SBBN-partner of $(\alpha X^-) + d \rightarrow {}^6\text{Li} + X^-$ but that of $(\alpha X^-) + d \rightarrow ({}^6\text{Li} X^-) + \gamma$. There is no SBBN-partner of $(\alpha X^-) + d \rightarrow {}^6\text{Li} + X^-$.

nuclear polarizability. The contribution of the ‘resonant’ $({}^7\text{Be}_{\frac{1}{2}}-X^-)_{2s}$ state is then capable of enhancing the recombination rate by a factor of a few. Bird *et al.* reported two types of the results, *with* and *without* the $({}^7\text{Be}_{\frac{1}{2}}-X^-)_{2s}$ contribution, when they discussed about the abundance of ${}^7\text{Li}$ - ${}^7\text{Be}$ and the lifetime and the abundance of X^- particle.

In order to remove the above ‘nuclear uncertainty’ completely, we perform an $\alpha + {}^3\text{He} + X^-$ three-body calculation of the energy of $({}^7\text{Be}_{\frac{1}{2}}-X^-)_{2s}$. The three-body Hamiltonian is the same as that taken in §2 where we investigated the reaction $(\alpha X^-) + {}^3\text{He} \rightarrow {}^7\text{Be} + X^-$, but here we take into account the spin of ${}^3\text{He}$ and ${}^7\text{Be}$ using a spin dependent $\alpha - {}^3\text{He}$ potential to reproduce the energies of ${}^7\text{Be}_{\frac{3}{2}-}$ and ${}^7\text{Be}_{\frac{1}{2}-}$. We find that the r.m.s. charge radius differs only by 0.05 fm between ${}^7\text{Be}_{\frac{3}{2}-}$ and ${}^7\text{Be}_{\frac{1}{2}-}$. The three-body calculation determined the energy of $({}^7\text{Be}_{\frac{1}{2}}-X^-)_{2s}$ as -41 keV for $m_X \rightarrow \infty$, -20 keV for $m_X = 100$ GeV and -2 keV for $m_X = 50$ GeV with respect to the ${}^7\text{Be}_{\frac{3}{2}-} + X^-$ threshold. Therefore, we conclude that the $({}^7\text{Be}_{\frac{1}{2}}-X^-)_{2s}$ state never becomes a resonance in the process of (3·26). In Ref. 6), two types of calculations of the element abundance *with* and *without* the $({}^7\text{Be}_{\frac{1}{2}}-X^-)_{2s}$ resonance are reported, but the case *with* the resonance is not acceptable.

Application of the $\alpha + {}^3\text{He} + X^-$ three-body calculation to full processes of the recombination of ${}^7\text{Be}$ and X^- will be one of our future subjects since the nuclear transition between the ${}^7\text{Be}_{\frac{3}{2}-}$ and ${}^7\text{Be}_{\frac{1}{2}-}$ states due to X^- is an important factor of the recombination and it can unambiguously be treated by the three-body model.

§4. X^- -catalyzed three-body breakup reactions

The most effective reactions to destroy ${}^6\text{Li}$ and ${}^7\text{Li}$ in SBBN are

$${}^6\text{Li} + p \rightarrow \alpha + {}^3\text{He} + 4.02 \text{ MeV} , \quad (4.1)$$

$${}^7\text{Li} + p \rightarrow \alpha + \alpha + 17.35 \text{ MeV} . \quad (4.2)$$

which have large S -factors ($S(0) \sim 3$ MeV b and ~ 0.06 MeV b, respectively¹⁷⁾). Therefore, the corresponding CBBN three-body breakup reactions

$$({}^6\text{Li}X^-) + p \rightarrow \alpha + {}^3\text{He} + X^- + 3.22 \text{ MeV} , \quad (4.3)$$

$$({}^7\text{Li}X^-) + p \rightarrow \alpha + \alpha + X^- + 16.47 \text{ MeV} , \quad (4.4)$$

should be taken care of in BBN calculations^{*)}. But, explicit calculation of these CBBN processes is tedious and difficult because (i) the exit channel is of three-body breakup, (ii) at least, a four-body model in which ${}^6\text{Li}$ (${}^7\text{Li}$) is composed of $d + \alpha$ ($t + \alpha$) is needed, (iii) $d(t)$ in ${}^6\text{Li}$ (${}^7\text{Li}$) is to be picked up by the incoming proton to form ${}^3\text{He}$ (α), and (iv) it is tedious to determine reasonably all the three spin-dependent nuclear interactions appearing in the four-body model. Instead, a naive

^{*)} Since the kinetic energy of the exit channel is large, formation of the bound states ${}^7\text{Be}$, ${}^8\text{Be}$, (αX^-) and $({}^3\text{He}X^-)$ in (4·3) and (4·4) is not important and is not explicitly written there.

approximation often taken in BBN network calculations, for instance in Refs. 4), 12), is that the cross section of the CBBN reaction (4.3) may be given by a product of the observed S -factor of the SBBN-partner reaction (4.1) and the CBBN Coulomb barrier penetration factor in which the charge of the target is reduced by one unit due to X^- ; and similarly for (4.4).

In this section, we propose a more sophisticated and phenomenologically reasonable three-body model to implement the information of the SBBN cross section into the CBBN calculation in place of making an explicit calculation of (4.3) and (4.4). Firstly, we calculate the SBBN reactions (4.1) and (4.2). We do not explicitly treat the channel-coupling between the entrance and the exit channels. Instead, we employ only the entrance channel, say $(AX^-) + a$, and introduce a complex potential $V_{A-a}(r)$ between the particles A and a (here, $A = {}^6, {}^7\text{Li}$ and $a = p$):

$$V_{A-a}(r) = V_{A-a}^{(\text{real})}(r) + iV_{A-a}^{(\text{imag})}(r) \quad (4.5)$$

as is seen in the nuclear optical-model potentials. In this case, the absorption cross section in the elastic $A - a$ scattering gives just the reaction cross section because there is no other open channel than the entrance and exit channels of (4.1) and (4.2). We determine the potential $V_{A-a}(r)$ so as to reproduce the observed SBBN cross section (S -factor).

Secondly, we incorporate this potential $V_{A-a}(r)$ into the three-body Hamiltonian (2.9) of the $A + a + X^-$ system and solve the elastic scattering between (AX^-) and a , namely the elastic $({}^6, {}^7\text{Li}X^-) + p$ scattering. We consider that the absorption cross section obtained in this scattering calculation provides with the cross section of the CBBN reaction^{*)}.

The total wave function is written, similarly to (2.12), but without the exit channel as

$$\Psi_{JM} = \phi_{00}^{(1)}(\mathbf{r}_1) \chi_{JM}^{(1)}(\mathbf{R}_1) + \Psi_{JM}^{(\text{closed})}, \quad (4.6)$$

where $\phi_{00}^{(1)}(\mathbf{r}_1)$ stands for the $1s$ wave function of $({}^6, {}^7\text{Li}X^-)$ and $\chi_{JM}^{(1)}(\mathbf{R}_1)$ for the $({}^6, {}^7\text{Li}X^-) + p$ scattering wave. The scattering boundary condition imposed to $\chi_{JM}^{(1)}(\mathbf{R}_1) (\equiv \chi_J^{(1)}(R_1) Y_{JM}(\hat{\mathbf{R}}_1))$ is given by

$$\lim_{R_1 \rightarrow \infty} R_1 \chi_J^{(1)}(R_1) = u_J^{(-)}(k_1, R_1) - S_{1 \rightarrow 1}^J u_J^{(+)}(k_1, R_1). \quad (4.7)$$

Similarly to the previous sections, the second term of (4.6), $\Psi_{JM}^{(\text{closed})}$, stands for all the asymptotically vanishing three-body amplitudes that are not included in the first scattering term, and is expanded in terms of the eigenfunctions of the Hamiltonian (without the imaginary part of (4.5)) as

$$\Psi_{JM}^{(\text{closed})} = \sum_{\nu=1}^{\nu_{\text{max}}} b_{J\nu} \Phi_{JM, \nu}. \quad (4.8)$$

^{*)} More precisely, this absorption cross section, for instance, in the case of $({}^6\text{Li}X^-) + p$ scattering, includes transitions to the $(\alpha X^-) + {}^3\text{He}$, $({}^3\text{He}X^-) + \alpha$, and ${}^7\text{Be} + X^-$ channels which are possible in the presence of the X^- particle, but are of quite minor importance due to the much smaller phase space than that in the three-body breakup channel.

Using $S_{1 \rightarrow 1}^J$ in (4.7), we derive the reaction cross section as

$$\sigma_{\text{reac}} = \frac{\pi}{k_1^2} \sum_{J=0}^{\infty} (2J+1) (1 - |S_{1 \rightarrow 1}^J|^2). \quad (4.9)$$

This reaction (absorption) cross section is known to be expressed alternatively as

$$\sigma_{\text{reac}} = \frac{-2}{\hbar v_1} \langle \Psi_{JM} | V_{A-a}^{(\text{imag})}(r_2) | \Psi_{JM} \rangle. \quad (4.10)$$

These two types of σ_{reac} utilize the information of quite different parts of the three-body wave function, namely the information of the asymptotic part along \mathbf{R}_1 in the former expression and that of the internal part along \mathbf{r}_2 in the latter. Therefore, it is a severe test to see the agreement between the two types of σ_{reac} . We obtained a precise agreement between their numbers in four significant figures, which demonstrates the high accuracy of our three-body calculation.

4.1. Nuclear complex potential and Coulomb potential

We construct the complex potential*) (4.5) between ${}^6, {}^7\text{Li}$ and p so as to reproduce the observed low-energy S -factors of (4.1) and (4.2) (the adopted values in Ref. 17)). The shape of the potential is assumed as

$$V^{(\text{real})}(r) = V_0 [1 + \exp\{(r - R_0)/a_0\}]^{-1} + V_{\text{Li}-p}^{\text{C}}(r), \quad (4.11)$$

$$V^{(\text{imag})}(r) = W_0 [1 + \exp\{(r - R_I)/a_I\}]^{-1}. \quad (4.12)$$

The Coulomb potential $V_{\text{Li}-p}^{\text{C}}(r)$ is derived by assuming a Gaussian charge distribution for ${}^6\text{Li}$ (${}^7\text{Li}$) which reproduces the observed r.m.s. charge radius 2.54 fm (2.43 fm).³³⁾ The energies of (${}^6\text{Li}X^-$) and (${}^7\text{Li}X^-$) are -0.773 MeV and -0.854 MeV, respectively, and the r.m.s. radii are 4.61 fm and 4.16 fm, respectively, with $m_X = 100$ GeV.

i) ${}^6\text{Li} - p$ potential

The potential parameters are chosen as follows: $V_0 = -59.5$ MeV, $R_0 = 2.5$ fm and $a = 0.6$ fm for the odd state, $V_0 = 400$ MeV, $R_0 = 1.5$ fm and $a = 0.2$ fm for the even state as well as $W_0 = -5.0$ MeV, $R_I = 2.5$ fm and $a_I = 0.6$ fm for both states. The repulsive potential for the even state is introduced as a substitute of the Pauli principle to exclude the s -state (contribution from the d -state is negligible).

ii) ${}^7\text{Li} - p$ potential

The potential parameters are chosen as follows: $V_0 = -77.2$ MeV, $R_0 = 2.5$ fm and $a = 0.6$ fm for the odd state, $V_0 = 400$ MeV, $R_0 = 1.5$ fm and $a = 0.2$ fm for the even state, and $W_0 = -1.1$ MeV, $R_I = 2.5$ fm and $a_I = 0.6$ fm for the odd state and $W_0 = 0$ for the even state. The reason to set $W_0 = 0$ for the even state is that, in the reaction (4.4), the odd angular momentum between the two α 's is prohibited, and therefore the even state of the ${}^7\text{Li} - p$ relative motion is forbidden (${}^7\text{Li}$ has the odd parity). This explains why the observed S -factor of (4.4), $S(0) \sim 0.06$ MeV b, is much smaller than that of (4.3), $S(0) \sim 3$ MeV b.

*) We follow the same prescription as that employed in Ref. 40) to determine the nuclear fusion rate in a muonic molecule ($d\mu$) by using a complex potential between d and t .

4.2. Result for three-body breakup reactions

Calculated S -factors of the CBBN reactions (4.1) and (4.2) are shown in Figs. 9 and 10 together with those of the SBBN-partner reactions.¹⁷⁾ It is interesting to see that the CBBN/SBBN ratio of the S -factor is nearly $0.6 \sim 1$ in the Gamow-peak region in both figures. Also, the ratio was nearly $1 \sim 2$ in the previous case in Fig. 8. This suggests that the CBBN reaction cross section may be approximated, within the error of nearly factor 2, by a simple model in which the CBBN S -factor in (2.21) is replaced by the observed S -factor of the SBBN partner reaction but the Coulomb barrier penetration factor is kept the same as in CBBN.

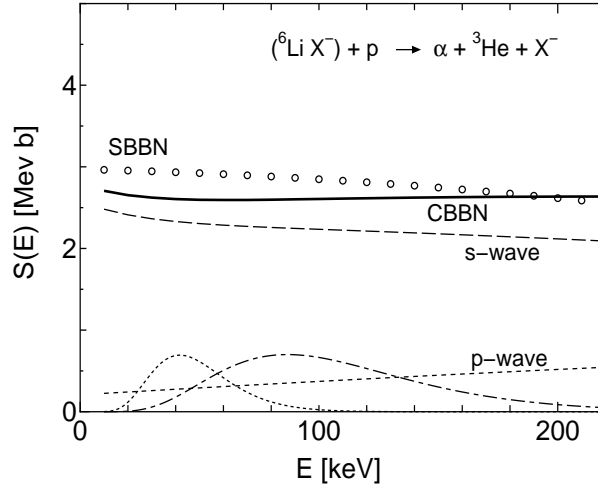


Fig. 9. The calculated S -factor for the CBBN reaction (4.1) (the solid line). The s - and p -wave contributions are shown individually. The observed S -factor of the SBBN partner reaction (4.3) is given in the open circles (the *adopted* values in Ref. 17)). The dotted curve illustrates the Gamow peak (in arbitrary units) for $T_9 = 0.1$ ($kT = 8.6$ keV) with the peak maximum at $E_0 = 42$ keV, and the dot-dashed curve is for $T_9 = 0.3$ ($kT = 26$ keV) with $E_0 = 87$ keV.

This simple model may be used in BBN network calculations (already employed in some literature calculations) when any precise CBBN reaction rate has not been available yet. But, the definition of the SBBN-partner reaction should be taken strictly as discussed in §3.5.

The S -factor of the CBBN reaction (4.1) in Fig. 9 may be simulated in the expression (2.27) as $S(E) \simeq 2.6 \times 10^3$ keV b. Using (2.28), the CBBN reaction rate is then given for $T_9 \lesssim 0.5$ as

$$N_A \langle \sigma v \rangle = 2.6 \times 10^{10} T_9^{-\frac{2}{3}} \exp(-6.74 T_9^{-\frac{1}{3}}) \text{ cm}^3 \text{ s}^{-1} \text{ mol}^{-1}. \quad (4.13)$$

In Fig. 10 for the reaction (4.2), the energy-dependence of $S(E)$ may be approximated by (2.27) with $S(0) = 36$ keV b and $\alpha = 0.15$ b, and therefore the reaction rate is written for $T_9 \lesssim 0.5$ as

$$N_A \langle \sigma v \rangle = 3.5 \times 10^8 T_9^{-\frac{2}{3}} \exp(-6.74 T_9^{-\frac{1}{3}}) (1 + 0.81 T_9^{\frac{2}{3}} + 0.30 T_9) \text{ cm}^3 \text{ s}^{-1} \text{ mol}^{-1}. \quad (4.14)$$

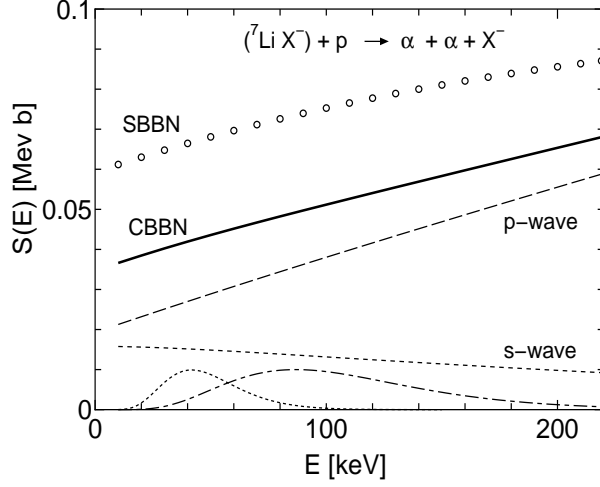


Fig. 10. The calculated S -factor for the CBBN reaction (4-2) (the solid line). The s - and p -wave contributions are shown individually. The observed S -factor of the SBBN partner reaction (4-4) is given in the open circles (the *adopted* values in Ref. 17)). The dotted curve is the Gamow peak (in arbitrary units) for $T_9 = 0.1$ ($kT = 8.6$ keV) with the peak maximum $E_0 = 42$ keV, and the dot-dashed curve is for $T_9 = 0.3$ ($kT = 26$ keV) with $E_0 = 87$ keV.

It will be interesting to see, in the BBN network calculation using the above reaction rates, whether the CBBN reactions (4-1) and (4-2) destroy significantly ${}^6,7\text{Li}$, since their SBBN partners (4-3) and (4-4) are the reactions that destruct ${}^6,7\text{Li}$ most strongly in standard BBN.

§5. X^- -catalyzed charge-exchange reactions

When the cosmic temperature cools to $T_9 \sim 0.01$, the X^- particle begins to form the *neutral* bound state*) (pX^-), if $\tau_X \gtrsim 10^6$ s; similarly, for (dX^-) and (tX^-) though their fraction is very much smaller (cf., for example, Fig. 2 of Ref. 12)). Owing to the *lack* of Coulomb barrier, the bound states are expected to interact strongly with other elements that have already been synthesized.

In this section, we perform a fully quantum three-body calculation of the following CBBN reactions that are induced by the neutral bound states (pX^-), (dX^-) and (tX^-):

a) Charge-exchange reactions,

$$(pX^-) + \alpha \rightarrow (\alpha X^-)_{3s,3p,3d} + p \quad (5.1)$$

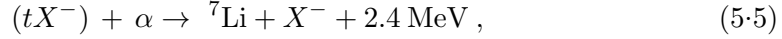
$$(dX^-) + \alpha \rightarrow (\alpha X^-)_{2s,2p} + d \quad (5.2)$$

$$(tX^-) + \alpha \rightarrow (\alpha X^-)_{2s,2p} + t \quad (5.3)$$

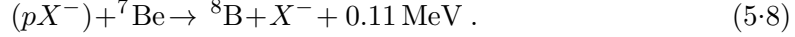
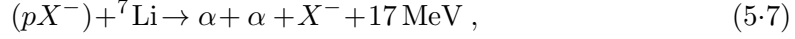
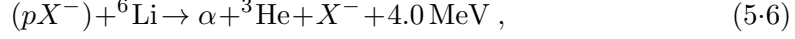
b) Reactions to produce ${}^6,7\text{Li}$,

$$(dX^-) + \alpha \rightarrow {}^6\text{Li} + X^- + 1.4 \text{ MeV} , \quad (5.4)$$

*) Binding energy of (pX^-) is ~ 0.025 MeV and the r.m.s. radius is ~ 50 fm.



c) Reactions to destroy ${}^6,{}^7\text{Li}$ and ${}^7\text{Be}$,

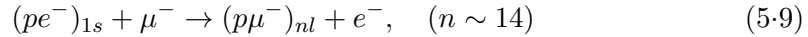


In the charge-exchange reactions, the excited states of the (αX^-) atom with the principal quantum numbers $n = 3$ and 2 are respectively employed in (5.1) and (5.2)–(5.3). They have the minimum transferred energy among the energetically possible $(\alpha X^-)_{nl}$ states.*)

Making a DWBA calculation, Jedamzik^{9),10)} insisted that the cross sections of the CBBN reactions (5.6) and (5.8) to destroy ${}^6\text{Li}$ and ${}^7\text{Be}$, respectively, are so large that (pX^-) could induce a second round of BBN, say late-time BBN, capable of destroying most of the previously synthesized ${}^6\text{Li}$ and ${}^7\text{Be}$. But, since the strength of the nuclear interactions (an order of ~ 10 MeV) that causes the reactions (5.6) and (5.8) is extremely larger than the incident energy ($\lesssim 1$ keV), the Born approximation should not be applied to these low-energy reactions.

Since the neutral bound state in the entrance channel behaves like a neutron at large distance with no Coulomb barrier, the reactions (5.4)–(5.8) caused by the nuclear interaction is expected to have much enhanced cross sections even at low energies (< 1 keV). Therefore, the most interesting issue in this section is whether or not the charge-exchange reactions are so strong that they can intercept the reactions (5.4)–(5.8) which work to produce and destroy Li and Be.

Before performing a precise quantum three-body calculation, we make a simple consideration, following the semiclassical approach in Refs. 14) and 41), in order to compare the cross section of the *atomic* process (5.1) with that of the *nuclear* reactions (5.4)–(5.8). In an analogy to the charge-exchange reactions seen in atomic physics, such as muon capture by a hydrogen⁴¹⁾



we understand that, if the incident α particle in (5.1) comes inside the proton $1s$ orbit of (pX^-) , sum of the inner charges seen by the proton becomes positive ($+e$), and therefore the proton escapes immediately from the orbit and instead the α particle is trapped by X^- as long as the incident energy is not too high. In the limit of the semiclassical picture, the cross section of (5.1) is approximately πb^2 , b being the r.m.s. radius of the (pX^-) atom ($b = 50.4$ fm). On the other hand, the cross section of the nuclear reaction is roughly πb_0^2 , b_0 being sum of the radius of the incoming nucleus and the nuclear interaction range ($b_0 \sim$ several fm). Therefore, the atomic cross section is roughly two orders of magnitude larger than the nuclear cross section. Actually, this picture is not fully applicable because the quantum effect is large for

*) Energies of the $1s$ state of (pX^-) , (dX^-) and (tX^-) are -25 keV, -48 keV and -71 keV, respectively, whereas those of $(\alpha X^-)_{nl}$ are -337 keV($1s$), -96 keV($2p$), -90 keV($2s$), -43 keV($3d$), -43 keV($3p$) and -41 keV($3s$).

the low-lying orbits with $n \leq 3$. But, we find that the following quantum three-body calculations give roughly a similar ratio of the two cross sections though each shows a strong energy dependence contrary to the above simple consideration.

a) Charge-exchange reactions

The method to calculate the cross sections of the charge-exchange reactions (5.1)–(5.3) is almost the same as Eqs.(2.8)–(2.20). For instance, for the reaction (5.1), the entrance channel (pX^-) + α is taken care by the Jacobi coordinate set $c = 1$ in Fig. 1, whereas the exit channel $(\alpha X^-)_{nl} + p$ is by $c = 3$. As for the closed-channel amplitude $\Psi_{JM}^{(\text{closed})}$ in (2.14), we take the same prescription as in §2.4. The Coulomb potentials are constructed by assuming the Gaussian charge distribution of p, d, t and α , which is the same as in the previous sections. Nuclear interactions play a negligible role in those atomic processes.

b) Reactions to produce Li

The α -transfer reactions (5.4) and (5.5) have the same structure as in (2.2) and (2.4), respectively. Therefore, the method for calculating cross sections of the former reaction is the same as that in §2 except that the entrance channel here is described by using the Jacobi coordinate set $c = 3$ in Fig. 1.

c) Reactions to destroy Li and Be

The two reactions (5.6) and (5.7) have the same structure as in (4.3) and (4.4), respectively. Then, the prescription to calculate them is the same to each other. The structure of the reaction (5.8) is similar to that of (3.2) though ${}^8\text{B}$ and X^- are not in a bound state here but in a photonless scattering state. In (3.2), the transition from the entrance channel to the exit one via the electromagnetic interaction was treated perturbatively, but the reaction (5.8) is solved as a ${}^7\text{Be} + p + X^-$ three-body problem.

5.1. Results

Calculated cross sections $\sigma(E)$ of reactions (5.1)–(5.8) are listed in Table II for the energies $E = 0.01, 0.1, 1$ and 10 keV ($T_9 \sim 0.0001, 0.001, 0.01$ and 0.1 , respectively). Since the Coulomb barrier penetration factor $\exp(-2\pi\eta(E))$ in (2.21) is unity here, the astrophysical S -factor is simply given by $S(E) = E\sigma(E)$.

Extreme enhancement of the cross sections of the reactions (5.4)–(5.8) due to the neutral bound states is seen, for example, in the fact that the ${}^6\text{Li}$ -production cross section of (5.4) at $E = 10$ keV is 6.4×10^{-1} b whereas that of (2.2) with (αX^-) in the entrance channel is 3.9×10^{-6} b.⁵⁾ As is seen in the usual *neutron*-induced low-energy reactions, the cross sections follows roughly the $1/v$ law in the lower energies ($\lesssim 1$ keV) in Table II.

The most important result in Table II is that the cross sections of the charge-exchange reactions are much larger than those of the nuclear reactions (5.4)–(5.8). Therefore, as for the α -transfer reactions (5.4) and (5.5), we understand that the bound states (dX^-) and (tX^-) are mostly changed to (αX^-) before producing ${}^6,7\text{Li}$. As for the Li-Be destruction reactions (5.6)–(5.8), we further note that the probability for (pX^-) to meet ${}^6,7\text{Li}$ and ${}^7\text{Be}$ is more than several orders of magnitude

Table II. Calculated cross sections and reaction rates of the late-time BBN reactions induced by the neutral bound states. The rates (in units of $\text{cm}^3 \text{s}^{-1} \text{mol}^{-1}$) are available for $T_9 \lesssim 0.05$.

Reaction	cross section (b)				reaction rate
	0.01 keV	0.1keV	1 keV	10 keV	
a) charge-exchange reaction					
$(pX^-) + \alpha \rightarrow (\alpha X^-)_{3\ell} + p$	8.4×10^3	2.2×10^3	7.8×10^2	7.5×10^1	1.0×10^{10}
$(dX^-) + \alpha \rightarrow (\alpha X^-)_{2\ell} + d$	3.1×10^3	9.1×10^2	2.0×10^2	2.1×10^1	3.5×10^9
$(tX^-) + \alpha \rightarrow (\alpha X^-)_{2\ell} + t$	8.3×10^3	1.9×10^3	3.2×10^2	2.5×10^1	7.6×10^9
b) α -transfer reaction					
$(dX^-) + \alpha \rightarrow {}^6\text{Li} + X^-$	9.6×10^0	3.0×10^0	6.9×10^{-1}	6.4×10^{-1}	1.1×10^7
$(tX^-) + \alpha \rightarrow {}^7\text{Li} + X^-$	3.5×10^{-1}	1.1×10^{-1}	2.7×10^{-2}	3.0×10^{-2}	4.3×10^5
c) Li-Be destruction					
$(pX^-) + {}^6\text{Li} \rightarrow \alpha + {}^3\text{He} + X^-$	1.8×10^2	5.5×10^1	1.1×10^1	2.8×10^0	1.6×10^8
$(pX^-) + {}^7\text{Li} \rightarrow \alpha + \alpha + X^-$	3.8×10^0	1.7×10^0	7.7×10^{-1}	1.6×10^{-1}	5.5×10^6
$(pX^-) + {}^7\text{Be} \rightarrow {}^8\text{B} + X^-$	4.8×10^{-1}	3.2×10^0	5.3×10^{-1}	5.5×10^{-2}	5.2×10^6

smaller than that to meet the α particle due to the large difference in the element abundances, and that, even if $(pX)^-$ had a chance to collide with an element A ($= {}^6, {}^7\text{Li}$ or ${}^7\text{Be}$), it would happen that another atomic charge-exchange reaction

$$(pX^-) + A \rightarrow (AX^-)_{nl} + p, \quad (A = {}^6, {}^7\text{Li}, {}^7\text{Be}) \quad (5.10)$$

intercepts immediately the reactions (5.6)–(5.8) since the cross section of (5.10) would be so large as in (5.1) though not being calculated here.

As a conclusion we understand that the nuclear reactions (5.4)–(5.8) to produce and destroy Li and Be would negligibly change the element abundance in the late-time BBN due to the strong interception by the charge-exchange reactions (5.1)–(5.3) and (5.10).

For the use in the network BBN calculation, we derive reaction rates of (5.1)–(5.8) under the approximation that the cross sections in Table II may roughly be simulated in a simple form (the $1/v$ law)

$$\sigma(E) \approx C/\sqrt{E}. \quad (5.11)$$

An evident reduction from (5.11) is seen at $E \gtrsim 10$ keV due to the structure of the neutral bound state and also the decreased probability of trapping the α particle by X^- , but the deviation would affect little on the element abundance*). Use of this approximation in the calculation of the reaction rate (2.23) makes the result

*) Also, the cross section at $E = 0.01$ keV in the bottom line of Table II is much smaller than (5.11), but this is because the p -wave contribution is dominant in (5.8) and the momentum matching becomes difficult at the low energies when the proton is transferred to a definite bound state in the exit channel.

constant^{*)} with respect to the temperature $T_9 \lesssim 0.05$:

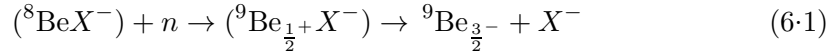
$$N_A \langle \sigma v \rangle = 2.6 \times 10^7 \sqrt{E_m/\mu} \sigma(E_m) \quad \text{cm}^3 \text{s}^{-1} \text{mol}^{-1}, \quad (5.12)$$

where the constant C is determined by matching (5.11) to $\sigma(E)$ in Table II at $E = E_m$. Here, E_m and $\sigma(E_m)$ are expressed in units of keV and b, respectively, and μ is the reduced mass of the entrance channel in units of amu. We then have simply averaged the three rates determined at $E_m = 0.01, 0.1$ and 1 (keV).

The calculated reaction rates are listed in the last column of Table II. We consider that it is not necessary to simulate $\sigma(E)$ in more sophisticated manner than (5.11) because it is clearly known from Table II and the discussion above that the late-time BBN does not affect the element abundances meaningfully^{**)}. A similar conclusion about the effect of the late-time BBN was obtained in Ref. 14).

§6. X^- -catalyzed production of ${}^9\text{Be}$

Absence of stable isotopes with mass number 8 is a bottle-neck for production of ${}^9\text{Be}$ and heavier nuclei in standard BBN. In recent papers,^{13),14)} Pospelov and his collaborators pointed out a possibility of enormous enhancement of the reaction rate to produce ${}^9\text{Be}$ by considering an X^- -catalyzed resonant neutron-capture process



and claimed that the primordial abundance of ${}^9\text{Be}$ imposes strong restrictions on the lifetime and the abundance of X^- . Here, ${}^9\text{Be}_{\frac{3}{2}^-}$ is the ground state and ${}^9\text{Be}_{\frac{1}{2}^+}$ denotes the first excited state with spin $\frac{1}{2}^+$ at $E_x = 1.735 \pm 0.003$ MeV with the neutron decay width $\Gamma_n = 0.225 \pm 0.012$ MeV⁴³⁾ (or $E_x = 1.684 \pm 0.007$ MeV with $\Gamma_n = 0.225 \pm 0.012$ MeV⁴⁴⁾).

In this section, we make an critical comment on this work.^{13),14)} Their attention to the reaction (6.1) is interesting, but there is a serious problem in their calculation. They assumed both the r.m.s. charge radius of ${}^8\text{B}$ and that of ${}^9\text{Be}$ to be 2.50 fm. Since the observed charge radius of ${}^9\text{Be}_{\frac{3}{2}^-}$ is 2.519 ± 0.012 fm,⁴⁴⁾ the assumed radius is acceptable for ${}^9\text{Be}_{\frac{3}{2}^-}$. But, there is no reason to take 2.50 fm for ${}^8\text{Be}$ which is a resonance state at 0.0918 MeV above the $\alpha+\alpha$ threshold. Its radius is not determined experimentally and theoretical derivation is, in principle, not done definitely.

Since the width of this resonance is, however, very small (5.57 eV), the wave function is heavily attenuated by the Coulomb barrier, followed by an asymptotically-oscillating amplitude which is roughly three orders of magnitude smaller than that in the nuclear interaction region. Therefore, it is not meaningless to derive the r.m.s.

^{*)} Pospelov *et al.*¹⁴⁾ derived the rate as $\propto 1/\sqrt{T_9}$, but this is due to that they did not calculate the energy dependence of the cross section and assumed it to be constant with respect to the energy. Their value at $T_9 = 0.01$ is in the same order of magnitude as ours for $(pX^-) + \alpha \rightarrow (\alpha X^-)_{\text{exc.}} + p$.

^{**)} According to a BBN network calculation by Kusakabe⁴²⁾ with including the reaction rates in Table II, abundances of the bound states (pX^-) , (dX^-) and (tX^-) at $T_9 \lesssim 0.05$ is heavily reduced by a factor of $\sim 10^5$ from those obtained without the rates.

radius by using the resonance wave function except for the asymptotic part or by using the wave function obtained through the diagonalization of the Hamiltonian with appropriate L^2 -integrable basis functions; both methods result in almost the same radius as long as they give the same resonance energy.

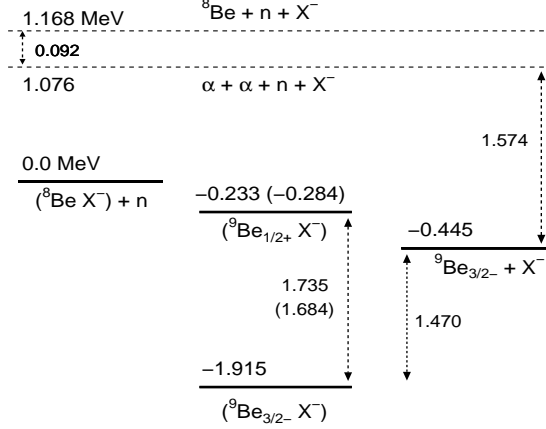


Fig. 11. Isobar diagram for the ${}^8\text{Be}+n+X^-$ system. This is to be compared with Fig. 1 of Ref. 13); here the same model as in Ref. 13) is employed but the r.m.s. charge radius of ${}^8\text{Be}$ is changed to an appropriate value from the radius used in Ref. 13)(see text). It is demonstrated that the $({}^9\text{Be}_{\frac{1}{2}+}X^-)$ state becomes *below* the $({}^8\text{Be}X^-) + n$ threshold contrary to Ref. 13).

A microscopic $\alpha+\alpha$ model calculation with the resonating group method (RGM) by Arai *et al.*⁴⁵⁾ gives 3.16 fm for the r.m.s. charge radius of ${}^8\text{Be}$ but the resonance is at 0.022 MeV above the $\alpha+\alpha$ threshold. A similar calculation with the orthogonality-condition model (OCM)²⁸⁾ by the present authors and their collaborators⁴⁶⁾ provides with 3.39 fm when the $\alpha+\alpha$ resonance is at the observed position 0.092 MeV. Since the latter model gives 3.20 fm when the resonance energy is tuned to be the same (0.022 MeV) as in the former RGM calculation, we here employ the r.m.s. charge radius of ${}^8\text{Be}$ to be 3.39 fm.

We now repeat the same analysis as in Refs. 13) and 14) taking the same model but the charge radii of 3.39 fm and 2.52 fm for ${}^8\text{Be}$ and ${}^9\text{Be}$, respectively. Here, $m_X \rightarrow \infty$ is taken as in Ref. 13). As is illustrated in Fig. 11, binding energies of $({}^8\text{Be}X^-)$ and $({}^9\text{Be}_{\frac{3}{2}-}X^-)$ are respectively 1.168 MeV and 1.470 MeV measured from the ${}^8\text{Be} + X^-$ threshold and ${}^9\text{Be}_{\frac{3}{2}-} + X^-$ one which is located by 1.574 MeV below the $\alpha + \alpha + n + X^-$ threshold. If we assume, according to Ref. 13), that ${}^9\text{Be}_{\frac{1}{2}+}$ has the same charge radius as ${}^9\text{Be}_{\frac{3}{2}-}$, we have the $({}^9\text{Be}_{\frac{1}{2}+}X^-)$ state just by 1.735 MeV⁴³⁾ (or 1.684 MeV⁴⁴⁾ above $({}^9\text{Be}_{\frac{3}{2}-}X^-)$. As a result we find that $({}^9\text{Be}_{\frac{1}{2}+}X^-)$ is not a resonance state but a bound state located by 0.233 MeV (0.284 MeV) *below* the $({}^8\text{Be}X^-) + n$ threshold with no neutron decay width (though the state has a small

width to make a particle decay to the ${}^9\text{Be}_{\frac{3}{2}-} + X^-$ channel). Those level energies depend on the shape of the charge distributions of ${}^8\text{Be}$ and ${}^9\text{Be}$, but the effect on the energy *difference* between the $({}^9\text{Be}_{\frac{1}{2}+}X^-)$ state and the $({}^8\text{Be}X^-) + n$ threshold is very small; for example, the difference changes only by 0.005 MeV if the charge distribution is artificially changed to Gaussian to square in both the nuclei. We then conclude that the resonant neutron-capture process (6.1) is not realized as long as the same model of Ref. 13) is employed.

Another problem in the analysis in Refs. 13), 14) is that the charge radius of the excited resonance state ${}^9\text{Be}_{\frac{1}{2}+}$ is assumed to be the same as that of the ground state ${}^9\text{Be}_{\frac{3}{2}-}$. An $\alpha + \alpha + n$ three-body RGM calculation by Arai *et al.*⁴⁵⁾ gives 2.88 fm for the r.m.s. charge radius of ${}^9\text{Be}_{\frac{1}{2}+}$. The calculated energy is ~ 0.4 MeV above the $\alpha + \alpha + n$ threshold while the observed value is 0.161 MeV⁴³⁾ (0.110 MeV⁴⁴⁾). Calculated neutron-decay width of ~ 0.2 MeV almost reproduces the experimental value. According to Arai,⁴⁵⁾ an artificial change of the resonance position, even down to slightly below the $\alpha + \alpha + n$ threshold (by tuning a part of the interaction), affects little on the charge radius of ${}^9\text{Be}_{\frac{1}{2}+}$; this is because the wave-function change is seen dominantly in the resonating valence neutron but little in the α clusters. If we employ the charge radius of 2.88 fm for ${}^9\text{Be}_{\frac{1}{2}+}$, the energy -0.233 MeV (-0.284 MeV) of $({}^9\text{Be}_{\frac{1}{2}+}X^-)$ shown in Fig. 11 is to be replaced by -0.116 MeV (-0.167 MeV). Therefore, consideration on the differences in the r.m.s. charge radii among ${}^8\text{Be}$, ${}^9\text{Be}_{\frac{3}{2}-}$ and ${}^9\text{Be}_{\frac{1}{2}+}$ still makes the $({}^9\text{Be}_{\frac{1}{2}+}X^-)$ state lying below the $\alpha + \alpha + n$ threshold.

In the above discussions on (6.1), it is still missing to consider the structure change of the *loosely-coupling* systems ${}^8\text{Be}$ and ${}^9\text{Be}_{\frac{1}{2}+}$ induced by the addition of the X^- particle to them. This dynamics can only be studied by employing an $\alpha + \alpha + n + X^-$ four-body model^{*)}. Use of this model also makes it possible to calculate exactly the $({}^8\text{Be}X^-)$ formation processes $\alpha + X^- \rightarrow (\alpha X^-) + \gamma$, $(\alpha X^-) + \alpha \rightarrow ({}^8\text{Be}X^-) + \gamma$ and the resonant (non-resonant) ${}^9\text{Be}_{\frac{3}{2}-}$ formation process (6.1). This study based on the four-body model is beyond the scope of the present paper, but is in progress to appear in the near future.

§7. Summary

(1) Using a fully quantum three-body method,¹⁸⁾ we have calculated the cross sections of various types of the big-bang nucleosynthesis (BBN) reactions that are catalyzed by a hypothetical long-lived negatively-charged, massive leptonic particle (called X^-) such as a supersymmetric (SUSY) particle *stau*, and provided their reaction rate for the use in the BBN network calculation. The rates are summarized

^{*)} This type of structure change by the injection of an impurity particle into loosely-coupling nuclear states has well been studied in light hypernuclei by the present authors and their collaborators⁴⁶⁾⁻⁴⁹⁾ by means of three- and four-body models.

in Table III and in the last column of Table II (the late-time BBN reactions for $T_9 \lesssim 0.05$).

(2) In the catalyzed BBN (CBBN) reactions, the strength of the nuclear interaction (of the order of 10 MeV) which causes the transition between the entrance and exit channels is very much larger than the incident energy ($\lesssim 200$ keV), and therefore the coupling between the two channels is so strong as to induce multi-step transitions between the channels. Therefore, any calculational method that does not take into account the above property of the interaction is not suited for application to the reactions. Also, for the charge-exchange reactions (5.1)–(5.3), a fully quantum, non-perturbative treatment is highly desirable since the α -particle is transferred to the low-lying states with the principal quantum number $n = 2 - 3$. We have shown that our three-body calculational method¹⁸⁾ satisfies the above requirements and is useful for the study of all the reactions.

(3) In the typical photonless CBBN reactions a)–c) in Table III, the calculated S -factors have similar orders of magnitude to those of the typical non-resonant photonless reactions in standard BBN (SBBN). As was first pointed by Pospelov¹⁾ and then confirmed by Hamaguchi *et al.*,⁵⁾ the S -factor of the CBBN reaction a) to produce ${}^6\text{Li}$ is many orders of magnitude larger than that of the radiative capture $\alpha + d \rightarrow {}^6\text{Li} + \gamma$ in SBBN. This imposes strong restrictions on the lifetime and the abundance of X^- . But, this large enhancement is simply because this SBBN reaction is heavily E1-hindered. On the other hand, the S -factors of the CBBN reactions b) and c) are found to be only by ~ 30 times larger than those of the strong E1 radiative capture SBBN reactions $\alpha + t({}^3\text{He}) \rightarrow {}^7\text{Li}({}^7\text{Be}) + \gamma$. Therefore, the reactions b) and c) do not seem to change the abundances of ${}^7\text{Li}$ – ${}^7\text{Be}$ meaningfully.

Table III. Summary of the calculated reaction rates of CBBN reactions obtained by the three-body calculation. The first three are for $T_9 \lesssim 0.2$ and the others are for $T_9 \lesssim 0.5$.

Reaction	Reaction rate ($\text{cm}^3 \text{s}^{-1} \text{mol}^{-1}$)	
<i>non-resonant reaction</i>		
a) $(\alpha X^-) + d \rightarrow {}^6\text{Li} + X^-$	$2.78 \times 10^8 T_9^{-\frac{2}{3}} \exp(-5.33 T_9^{-\frac{1}{3}})(1 - 0.62 T_9^{\frac{2}{3}} - 0.29 T_9)$	
b) $(\alpha X^-) + t \rightarrow {}^7\text{Li} + X^-$	$1.4 \times 10^7 T_9^{-\frac{2}{3}} \exp(-6.08 T_9^{-\frac{1}{3}})(1 + 1.3 T_9^{\frac{2}{3}} + 0.55 T_9)$	
c) $(\alpha X^-) + {}^3\text{He} \rightarrow {}^7\text{Be} + X^-$	$9.4 \times 10^7 T_9^{-\frac{2}{3}} \exp(-9.66 T_9^{-\frac{1}{3}})(1 + 0.20 T_9^{\frac{2}{3}} + 0.05 T_9)$	
d) $({}^6\text{Li}X^-) + p \rightarrow \alpha + {}^3\text{He} + X^-$	$2.6 \times 10^{10} T_9^{-\frac{2}{3}} \exp(-6.74 T_9^{-\frac{1}{3}})$	
e) $({}^7\text{Li}X^-) + p \rightarrow \alpha + \alpha + X^-$	$3.5 \times 10^8 T_9^{-\frac{2}{3}} \exp(-6.74 T_9^{-\frac{1}{3}})(1 + 0.81 T_9^{\frac{2}{3}} + 0.30 T_9)$	
f) $({}^7\text{Be}X^-) + p \rightarrow ({}^8\text{B}X^-) + \gamma$	$2.3 \times 10^5 T_9^{-\frac{2}{3}} \exp(-8.83 T_9^{-\frac{1}{3}})(1 + 1.9 T_9^{\frac{2}{3}} + 0.54 T_9)$	
<i>resonant reaction</i>		
g) $({}^7\text{Be}X^-) + p \rightarrow ({}^8\text{B}X^-)_{2p}^{\text{res.}}$	$1.37 \times 10^6 T_9^{-\frac{3}{2}} \exp(-2.28 T_9^{-1})$	$m_X = 50\text{GeV}$
$\rightarrow ({}^8\text{B}X^-) + \gamma$	$1.44 \times 10^6 T_9^{-\frac{3}{2}} \exp(-2.15 T_9^{-1})$	$m_X = 100\text{GeV}$
	$1.48 \times 10^6 T_9^{-\frac{3}{2}} \exp(-2.04 T_9^{-1})$	$m_X = 500\text{GeV}$
	$1.51 \times 10^6 T_9^{-\frac{3}{2}} \exp(-2.01 T_9^{-1})$	$m_X \rightarrow \infty$

(4) The resonant radiative-capture CBBN reaction, (g) in Table III (cf. Fig. 5), was proposed by Bird *et al.*⁶⁾ as a possible solution to the ${}^7\text{Li}$ - ${}^7\text{Be}$ overproduction. We have examined their model and result by means of a ${}^7\text{Be} + p + X^-$ three-body model which makes it possible to calculate all the steps in the reaction. We have shown that both the very-loosely-coupling ${}^7\text{Be} + p$ structure of ${}^8\text{B}$ and the strongly spin-dependent ${}^7\text{Be}_{\frac{3}{2}^-} - p$ interaction contribute largely to the energy of the resonance $({}^8\text{B}X^-)_{2p}^{\text{res.}}$. But, the effects work oppositely almost cancelling to each other, and therefore the reaction rate by the simple model⁶⁾ (assuming a Gaussian charge distribution of ${}^8\text{B}$) is by chance close to ours. The rate is sensitive to m_X ; the rate with $m_X = 100$ GeV is 60% of that with $m_X \rightarrow \infty$ at $T_9 = 0.3$.

As for the recombination process to form $({}^7\text{Be}_{\frac{3}{2}^-}X^-)$ starting from ${}^7\text{Be}_{\frac{3}{2}^-}$ and a proton, we pointed out in §3.6 that their calculation⁶⁾ of the energy of the ‘resonance’ state $({}^7\text{Be}_{\frac{1}{2}^-}X^-)_{2s}$ is erroneous due to the absence of consideration on the nuclear structure of ${}^7\text{Be}_{\frac{3}{2}^-}$ and ${}^7\text{Be}_{\frac{1}{2}^-}$; the $\alpha + {}^3\text{He} + X^-$ three-body calculation made clear that the $({}^7\text{Be}_{\frac{1}{2}^-}X^-)_{2s}$ state cannot be a resonance but a bound state below the ${}^7\text{Be}_{\frac{3}{2}^-} + X^-$ threshold. Ref. 6) reported two types of results on the abundance of ${}^7\text{Li}$ - ${}^7\text{Be}$ calculated *with* and *without* the $({}^7\text{Be}_{\frac{1}{2}^-}X^-)_{2s}$ resonance, but the case *with* the resonance is not acceptable.

(5) We have studied fully quantum mechanically the late-time BBN reactions (5.1)–(5.8) which take place at $T_9 \lesssim 0.01$ between the neutral bound states, (pX^-) , (dX^-) and (tX^-) , and light nuclei. The atomic charge-exchange reactions (5.1)–(5.3) are so dominant that they immediately intercept the nuclear reactions (5.4)–(5.8). Therefore, we conclude that change of element abundances due to the late-time BBN reactions is negligible.

(6) We have examined the resonant neutron-capture CBBN process (6.1) to produce ${}^9\text{Be}$ proposed by Pospelov *et al.*^{13),14)} They claimed that the resulting increased output of ${}^9\text{Be}$ constrains strongly the abundance and the lifetime of X^- . But, we found that, as long as the same model of Ref. 13) is employed but with an appropriate charge radius of ${}^8\text{Be}$ being taken (a too small value of the radius was used in Ref. 13)), the intermediate state $({}^9\text{Be}_{\frac{1}{2}^+}X^-)$ appears *below* the $({}^8\text{Be}X^-) + n$ threshold thus giving no resonant mechanism. The model is, however, too simple to account for the structure change of the *loosely-coupling* (resonant) systems ${}^8\text{Be}$ and ${}^9\text{Be}_{\frac{1}{2}^+}$ due to the injection of the X^- particle into them. Therefore, an extended four-body calculation based on an $\alpha + \alpha + n + X^-$ model is underway for examining (6.1) much more seriously.

(7) Finally, we expect that application of the presently-obtained reaction rates to the BBN network calculation will help to solve the ${}^6\text{Li}$ - ${}^7\text{Li}$ problem and simultaneously to impose restrictions on the primordial abundance and the lifetime of the X^- particle.

Acknowledgements

The authors would like to acknowledge helpful discussions with M. Kusakabe on the BBN network calculation and with K. Arai for the structure of ^8Be and ^9Be . They are also grateful to K. Hamaguchi, T. Hatsuda and T.T. Yanagida for valuable discussions on the stau-catalyzed BBN reactions. This work was supported in part by the Grant-in-Aid for Scientific Research from Monbukagakusho of Japan. The numerical calculations were performed on HITACHI SR11000 at KEK and FUJITSU PRIMEQUEST 580 at Kyushu University.

References

- 1) M. Pospelov, Phys. Rev. Lett. **98** (2007), 231301, hep-ph/0605215.
- 2) K. Kohri and F. Takayama, Phys. Rev. D **76** (2007), 063507, hep-ph/0605243.
- 3) M. Kaplinghat and A. Rajaraman, Phys. Rev. D **74** (2006), 103004, astro-ph/0606209.
- 4) R.H. Cyburt, J. Ellis, B.D. Fields, K.A. Olive and V.C. Spanos, J. Cosmology and Astroparticle Phys. **0611** (2006), 014, astro-ph/0608562.
- 5) K. Hamaguchi, T. Hatsuda, M. Kamimura, Y. Kino and T.T. Yanagida, Phys. Lett. **B650** (2007), 268, hep-ph/0702274.
- 6) C. Bird, K. Koopmans and M. Pospelov, Phys. Rev. D **78** (2008), 083010, hep-ph/0703096v3.
- 7) M. Kawasaki, K. Kohri and T. Moroi, Phys. Lett. B **649** (2007), 436, hep-ph/0703122.
- 8) T. Jittoh, K. Kohri, K. Koike, J. Sato, T. Shimomura and M. Yamanaka, Phys. Rev. D **76** (2007), 125023, hep-ph/0704.2914.
- 9) K. Jedamzik, Phys. Rev. D **77** (2008), 063524, astro-ph/0707.2070.
- 10) K. Jedamzik, J. Cosmology and Astroparticle Phys. **0803** (2008), 008, astro-ph/0710.5153.
- 11) M. Kusakabe, T. Kajino, R.N. Boyd, T. Yoshida and G. Mathews, Phys. Rev. D **76** (2007), 121302, astro-ph/0711.3854.
- 12) M. Kusakabe, T. Kajino, R. N. Boyd, T. Yoshida, and G. J. Mathews, Astrophys. J. **680** (2008), 846, astro-ph/0711.3858.
- 13) M. Pospelov, hep-ph/0712.0647.
- 14) M. Pospelov, J. Pradler and F.D. Steffen, J. Cosmology and Astroparticle Phys. **0811** (2008), 026, hep-ph/0807.4287.
- 15) M. Asplund, D.L. Lambert, P.E. Nissen, F. Primas and V.V. Smith, Astrophys. J. **644** (2006), 229, astro-ph/0510636.
- 16) For example, J.L. Feng and B.T. Smith, Phys. Rev. D **71** (2005), 015004; K. Hamaguchi, M. Nojiri and A. de Roeck, J. High Energy Phys. **0703** (2007), 046.
- 17) C. Angulo *et al.*, Nucl. Phys. A **656** (1999), 3.
- 18) E. Hiyama, Y. Kino and M. Kamimura, Prog. Part. Nucl. Phys. **51** (2003), 223.
- 19) D.N. Spergel *et al.*, Astrophys. J. Suppl. **170** (2007), 377.
- 20) K. M. Nollett, R. B. Wiringa and R. Schiavilla, Phys. Rev. C **63** (2001), 024003.
- 21) M. Kamimura, Phys. Rev. **A38** (1988), 621.
- 22) M. Kamimura, Muon Catalyzed Fusion **3** (1988), 335.
- 23) Y. Kino and M. Kamimura, Hyperfine Interactions **82** (1993), 45.
- 24) K. Nagamine and M. Kamimura, Advanced in Nuclear Physics **24** (1998), 151.
- 25) M. Kamimura, Prog. Theor. Phys. Suppl. No. 62 (1977), 236.
- 26) D.D. Clayton, *Principles of Stellar Evolution and Nuclear Synthesis* (The University of Chicago Press, 1983).
- 27) K. Ikeda *et al.*, Prog. Theor. Phys. Suppl. **68** (1980), 1.
- 28) S. Saito, Prog. Theor. Phys. **41** (1969), 705.
- 29) Y. Kino, N. Yamanaka, M. Kamimura, and H. Kudo, Interactions **146/147** (2003), 331.
- 30) W.-M. Yao *et al.* (Particle Data Group), J. Phys. G **33** (2006), 1.
- 31) M. Hori *et al.*, Phys. Rev. Lett. **91** (2003), 123401.
J. Cosmology and Astroparticle Phys. **12**
- 32) M. Kawasaki, K. Kohri and T. Moroi, Phys. Rev. D **71** (2005), 083502.
- 33) I. Tanihata *et al.*, Phys. Rev. Lett., **55** (1985), 2676.

- 34) I. Tanihata *et al.*, Phys. Lett., B **206** (1988), 592.
- 35) P. Descouvemont and D. Bay, Nucl. Phys. A **567** (1994), 341.
- 36) K. Varga, Y. Suzuki and I. Tanihata, Phys. Rev. C **52** (1995), 3013.
- 37) A. Cs6t6 and K. Langanke, Nucl. Phys. A **636**, (1998) 240.
- 38) H. Esbenson, Phys. Rev. C **70** (2004), 047603.
- 39) K. Ogata, S. Hashimoto, Y. Iseri, M. Kamimura, M. Yahiro, Phys. Rev. C **73** (2006), 024605.
- 40) M. Kamimura, AIP Conference Proceedings **181** (1989), 330.
- 41) J. Cohen, Phys. Rev. A **27** (1983), 167.
- 42) M. Kusakabe, private communication (2008).
- 43) K. Sumiyoshi, H. Utsunomiya, S. Goko and T. Kajino, Nucl. Phys. A **709** (2002), 467.
- 44) D.R. Tilley *et al.*, Nucl. Phys. A **745** (2004), 155.
- 45) K. Arai, P. Descouvemont, D. Baye and W.N. Catford, Phys. Rev. C **68** (2003), 014319.
K. Arai, Phys. Rev. C **69** (2004), 014309; private communication (2008).
- 46) E. Hiyama, M. Kamimura, T. Motoba, T. Yamada and Y. Yamamoto, Phys. Rev. C **66** (2002), 024007; private communication on the radius of ^8Be .
- 47) E. Hiyama, M. Kamimura, T. Motoba, T. Yamada and Y. Yamamoto, Prog. Theor. Phys. **97** (1997), 881.
- 48) E. Hiyama, M. Kamimura, K. Miyazaki and T. Motoba, Phys. Rev. C **59** (1999), 2351.
- 49) E. Hiyama, M. Kamimura, T. Motoba, T. Yamada and Y. Yamamoto, Phys. Rev. C **65** (2001), 011301(R).